NASA TECHNICAL NOTE

NASA TN D-5123

A RENDEZVOUS AND STATION-KEEPING SIMULATOR WITH FLY-AROUND CAPABILITY AND VIRTUAL-IMAGE VIEWING

by William M. Kahlbaum, Jr., Richard E. Bardusch, and John J. Stumpf

Langley Research Center
Langley Station, Hampton, Va.

NATIONAL AERONAUTICS AND SPACE ADMINISTRATION • WASHINGTON, D. C. • APRIL 1969

A RENDEZVOUS AND STATION-KEEPING SIMULATOR WITH FLY-AROUND CAPABILITY AND VIRTUAL-IMAGE VIEWING

By William M. Kahlbaum, Jr., Richard E. Bardusch, and John J. Stumpf

Langley Research Center
Langley Station, Hampton, Va.

NATIONAL AERONAUTICS AND SPACE ADMINISTRATION

For sale by the Clearinghouse for Federal Scientific and Technical Information
Springfield, Virginia 22151 – CFSTI price $3.00

A RENDEZVOUS AND STATION-KEEPING SIMULATOR WITH FLY-AROUND CAPABILITY AND VIRTUAL-IMAGE VIEWING

By William M. Kahlbaum, Jr., Richard E. Bardusch, and John J. Stumpf
Langley Research Center

SUMMARY

A screen-type-refractive-virtual-image rendezvous simulator has been designed and built at the Langley Research Center. In this simulator, the test subject views combined images of a celestial background, a featureless earth horizon, and a rendezvous target vehicle through a circular window with a 30^{o} field of view. The virtual images of the horizon and stars appear to be at infinity, while the target-vehicle image appears to be at some closer distance. The three elements of the display are rear projected on screens by means of separate gimbaled projectors. The horizon and star images are generated optically, while the target-vehicle image is generated by a closed-circuit television system. The observed size of the target-vehicle image varies as a function of problem range. Range changes within 160 meters of the observer are simulated by moving the television camera along a range bed. Range changes beyond 160 meters with satisfactory television line resolution are simulated by continuously shrinking the raster on the television projection tube. Since the problem requires three degrees of continuous rotational freedom for the observer, a central computer program generates attitude information (by means of quaternion rate equations) and presents this information to the simulator in the form of direction cosine matrices. Special-purpose resolver computers are employed to convert the direction cosines into specific hardware gimbal angles.

This report describes the simulator equipment and gives particular attention to the raster shrinkage and gimbal-angle resolving techniques.

INTRODUCTION

A simulator has been developed at the Langley Research Center to provide a realistic visual display for use in rendezvous and station-keeping studies. The visual display furnishes the observer with a dynamic "out-the-window" scene consisting of a target-vehicle image, a featureless earth horizon, and a star-field background. Dynamic motion of the scene is achieved by means of gimbaled projection devices. A photograph of the

combined image of the horizon and target as viewed through the window is presented as figure 1. Further visual realism is achieved by the use of a screen-type-virtual-image viewing system.

The original intent in the development of this simulator was to investigate the optical characteristics of screen-type-virtual-image systems. Shortly after its construction, however, the system was adapted for use in rendezvous and station-keeping studies for the Gemini program. Although the overall system concept is not unique, two items of the equipment developed represent techniques which are considered to be of general interest and applicability in the field of simulation. The first is a raster shrinkage technique used with an 80-kilovolt, theater-type television projection system. The second is a technique for employing resolvers to convert direction cosines into gimbal position angles. This second technique is particularly attractive in that the resolver equipment can be programed easily for any order of gimbal rotation which may be required by the projection hardware and can provide continuous rotational freedom about all axes.

SYMBOLS

A	amplifier
a	radius of horizon mask, inches (meters)
a_{ij}	elements of 3-by-3 direction cosine matrix
b	distance from center of rotation of gimbaled mirror to projection screen, inches (meters)
C	capacitor
C_k	capacitance of any element k, microfarads
D	lateral displacement of target image on projection screen relative to system optic axis, inches (meters)
D'	lateral displacement of target virtual image relative to system optic axis, inches (meters)
d	distance from television projection lens to center of rotation of two-gimbal mirror, inches (meters)

E_c voltage appearing on capacitor C1, volts

E_{in} voltage output of amplifier A2 plus a bias voltage proportional to target range, volts

E_r voltage proportional to target range from central computer, volts

E_1 voltage output of amplifier A1, volts

E_2 voltage output of amplifier A2, volts

E_3 voltage output of amplifier A3, volts

e horizon-projector mask height, inches (meters)

f_c focal length of television camera lens, inches (meters)

f_p focal length of television projection lens, inches (meters)

f_v focal length of viewing lens, inches (meters)

g distance between television camera lens and image formed on face of vidicon, inches (meters)

H_o lateral dimension of horizon image on screen relative to system optic axis, inches (meters)

I current, amperes

J lateral dimension of real-world target relative to line of sight, feet (meters)

J' lateral dimension of target virtual image relative to system optic axis, inches (meters)

J_c lateral dimension of target model relative to camera optic axis, inches (meters)

J_c' lateral dimension of image of target model on face of television camera pickup tube, inches (meters)

J_p lateral dimension of target image on face of television projection tube, inches (meters)

J_p' lateral dimension of target image on projection screen, inches (meters)

K nominal distance from viewing lens to observer's eye position, inches (meters)

L distance from gimbal center of star projector to projection screen, inches (meters)

M distance from gimbal center of horizon projector to projection screen, inches (meters)

m lens magnification, dimensionless

m_e electronic magnification factor, dimensionless

n distance from television projection lens to target projection screen, inches (meters)

Q transistor

R resistor

R_k resistance of any element k, ohms

r target-to-observer range, feet (meters)

r' object distance between television camera lens and center of rotation of target-model gimbal, inches (meters)

S distance from projection screen to viewing lens, inches (meters)

S' distance from viewing lens to observed virtual image, inches (meters)

t time, seconds

y displacement of a projected star image on screen relative to system optic axis, inches (meters)

α	line-of-sight yaw angle, radians
α'	two-gimbal-mirror yaw drive angle, radians
β	line-of-sight pitch angle, radians
β'	two-gimbal-mirror pitch drive angle, radians
θ	observed angular displacement of a star relative to system optic axis, radians
θ_h	horizon-projector pitch gimbal angle, radians
θ_I	star-projector pitch gimbal angle, radians
θ_T	target-model pitch gimbal angle, radians
θ_o	observed horizon depression angle relative to system optic axis, radians
ϕ	angular displacement of a star on star projector sphere relative to system optic axis, radians
ϕ_h	horizon-projector roll gimbal angle, radians
ϕ_I	star-projector roll gimbal angle, radians
ϕ_T	target-model-image roll gimbal angle, radians
ϕ_o	angle subtended by horizon projector mask relative to system optic axis as measured at gimbal center of horizon projector, radians
ψ_h	horizon-projector yaw gimbal angle, radians
ψ_I	star-projector yaw gimbal angle, radians
ψ_T	target-model yaw gimbal angle, radians
$\hat{i}_1,\hat{j}_1,\hat{k}_1$	orthogonal unit vectors defining observer body-axis system X_1,Y_1,Z_1, dimensionless

$\hat{i}_2,\hat{j}_2,\hat{k}_2$ orthogonal unit vectors defining line-of-sight axis system X_2,Y_2,Z_2, dimensionless

$\hat{i}_3,\hat{j}_3,\hat{k}_3$ orthogonal unit vectors defining target body-axis system X_3,Y_3,Z_3, dimensionless

$\hat{i}_4,\hat{j}_4,\hat{k}_4$ orthogonal unit vectors defining observer local vertical-axis system X_4,Y_4,Z_4, dimensionless

$\hat{i}_5,\hat{j}_5,\hat{k}_5$ orthogonal unit vectors defining star-field (inertial) axis system X_5,Y_5,Z_5, dimensionless

μ amplifier open-loop gain, dimensionless

DESCRIPTION OF OVERALL SYSTEM

The physical system consists of two vehicles (the observer and the target) each of which is represented in the computer mathematical model by equations of motion in six degrees of freedom. Figure 2 illustrates the angular relationships between the several axis systems which describe the physical system. The simulation employs a fixed-base cockpit so that all scene motions must be derived relative to the observer body-axis system.

A block diagram of the entire simulator-computer system is presented as figure 3. The cockpit is equipped with an instrument panel and controllers with the pilot's controller deflections being fed to the computer as inputs to the equations of motion. The computer outputs generate the signals to drive the cockpit displays and projection systems, which form the images of the target, horizon, and star field. As shown in figure 3, the line-of-sight angles α and β are directly available from the computer program as inputs to the target positioning mirror. All other gimbal angles exist implicitly as elements of the direction cosine matrices representing the several axis transformations. Special-purpose resolver computers (Euler angle computers) are used in the conversion of the matrix elements to the required gimbal angles with the angular outputs generated in the form of shaft rotations. A synchro device attached to each shaft provides the position input information to the closed-loop servo drive on each projector gimbal. This method of generating the gimbal angles provides the fly-around capability which was required during the station-keeping portion of the simulation. The target image is generated by means of a closed-circuit television (T V) system. The range excursion of 10 meters to 3600 meters necessitated the use of a combination of physical camera

motion (range bed) and continuous shrinkage of the projection-tube raster to provide a properly scaled image with satisfactory line resolution at all range values.

VISUAL DISPLAY

Formation of Virtual Images

Figure 4 illustrates the projection and optical mixing of the star-field, horizon, and target-vehicle images. The images on the rear projection screens S1 and S2 are combined by means of beam splitter B2 and appear as a composite image to the observer. Screen S1, which displays the star-horizon scene, is located at the focal point of the viewing lens and, thus, a virtual image is formed at infinity. Screen S2, which displays the target image, is located between the lens and its focal point and, thus, a virtual image is formed at a predetermined finite distance. In either case, the apparent distance of the virtual image may be determined by using the following formula for a simple lens:

$$S' = \frac{Sf_V}{S - f_V} \tag{1}$$

where

S distance from projection screen to viewing lens

S' distance from viewing lens to observed virtual image

f_V focal length of viewing lens

Since the apparent distance of the target image is determined by the position of screen S2 relative to the focal point of the viewing lens, it would be preferable to vary this relationship as a function of target range in order to maintain the correct observed parallax. Although this capability does not exist in the equipment, screen S2 is equipped with a mechanism which allows the adjustment of the apparent image distance.

Star-Field-Image Generation

General description.- The star field from a point-light-source planetarium projector is imaged onto screen S1 after reflection from beam splitter B1. The planetarium projector contains a total of 1500 accurately positioned stars. Sixty of the brighter stars are projected optically by means of small lenses mounted in the surface of the sphere. The remaining stars are produced by small holes drilled in the sphere which allow the light from the point source to fall on the screen; star magnitudes are determined by the size of the holes. (See fig. 4.)

Motion.- The order of rotation of the star-field projector gimbals is ϕ_I, θ_I, ψ_I. As shown in figure 2(c), the orientation of the rotating star-field (inertial) axis system relative to the fixed-body axis system is specified by three Euler angle rotations: ϕ_I about the $\hat{i}_1$-axis, followed by θ_I about the intermediate $\hat{j}_1'$-axis, followed by ψ_I about the $\hat{k}_5$-axis. The resulting transformation is (see ref. 1)

$$\begin{bmatrix} X_5 \\ Y_5 \\ Z_5 \end{bmatrix} = \begin{bmatrix} c\theta_I c\psi_I & c\phi_I s\psi_I + s\phi_I s\theta_I c\psi_I & s\phi_I s\psi_I - c\phi_I s\theta_I c\psi_I \\ -c\theta_I s\psi_I & c\phi_I c\psi_I - s\phi_I s\theta_I s\psi_I & s\phi_I c\psi_I + c\phi_I s\theta_I s\psi_I \\ s\theta_I & -s\phi_I c\theta_I & c\phi_I c\theta_I \end{bmatrix} \begin{bmatrix} X_1 \\ Y_1 \\ Z_1 \end{bmatrix} \tag{2}$$

where c and s represent cosine and sine, respectively.

Projector geometry.- The angular relationships between the stars on the planetarium sphere must be preserved in the observed star-field image. The requirements which must be satisfied to guarantee this relationship are illustrated in figure 5. Consider two stars A and B which are separated by an angle ϕ on the sphere (star A is assumed to be coincident with the optic axis for simplicity). If it is assumed that all light rays from a given star emerge from the viewing lens parallel to each other, the following expressions can be written:

$$\tan \phi = \frac{y}{L} \tag{3}$$

$$\tan \theta = \frac{y}{f_v} \tag{4}$$

where θ is the observed angle between the two stars. The required condition for $\theta = \phi$ is that $L = f_v$ which specifies the distance of the star projector from the screen.

Horizon-Image Generation

General description.- Figure 6 illustrates the geometry involved in the projection of the horizon image. A point light source is mounted at the center of the cylindrical mask so that a shadow is formed on screen S1. The constant height of the horizon-projector mask e determines the depression angle and curvature of the horizon image on the screen. Relative motion of the horizon in roll and pitch is introduced by rotating the mask in a two-gimbal system.

Motion.- The order of rotation of the horizon projector gimbals is ϕ_h, θ_h. As shown in figure 2(d), the orientation of the rotating local vertical-axis system relative to the fixed-body axis system is specified by two Euler angle rotations: ϕ_h about the $\hat{i}_1$-axis followed by θ_h about the $\hat{j}_4$-axis. The third rotation ψ_h about the $\hat{k}_4$-axis is

not included since the horizon image contains no terrain features. The resulting transformation is

$$\begin{bmatrix} X_4 \\ Y_4 \\ Z_4 \end{bmatrix} = \begin{bmatrix} c\theta_h & s\phi_h s\theta_h & -c\phi_h s\theta_h \\ 0 & c\phi_h & s\phi_h \\ s\theta_h & -s\phi_h c\theta_h & c\phi_h c\theta_h \end{bmatrix} \begin{bmatrix} X_1 \\ Y_1 \\ Z_1 \end{bmatrix} \tag{5}$$

Projector geometry.- The observed depression angle of the horizon display is established by the height of the horizon-projector mask e with the required depression angle being determined by the desired altitude. This relationship is illustrated in figure 6 for $\theta_h = 0$. If it is assumed that all light rays from a given point on the horizon emerge from the viewing lens parallel to each other, the following expressions can be written:

$$H_o = f_v \tan \theta_o = M \tan \phi_o \tag{6}$$

or

$$\tan \phi_o = \frac{f_v}{M} \tan \theta_o \tag{7}$$

Also, from figure 6

$$\tan \phi_o = \frac{e}{a} \tag{8}$$

Combining equations (7) and (8) gives

$$\frac{e}{a} M = f_v \tan \theta_o$$

This expression determines the mask height and location for any desired depression angle.

Target-Vehicle-Image Generation and Display

General description.- The target-vehicle image projected on screen S2 is generated by means of a closed-circuit television system as illustrated in figure 7. The television pickup consists of the camera lens L3 and a vidicon pickup tube. The vidicon and its control unit operate at 675 lines per frame, 30 frames per second with a 2:1 interlace. The vidicon and its deflection yoke are mounted inside a servo-driven slip-ring assembly, the motion of which introduces the roll of the target image about the line of sight. The remaining two motions of the target vehicle relative to the line of sight are produced by the two gimbal rotations of the target model. The camera and slip-ring assembly are mounted on the movable carriage of a range bed. The size of the image formed on the face of the vidicon is proportional to r'. Proper focus is maintained by varying the effective focal length of the camera lens as a function of r'. Any value of target range

beyond the maximum limit of the range bed is simulated by varying the electronic magnification factor m_e in the projection electronics. The magnification factor is defined as

$$m_e = \frac{\text{Size of projection-tube raster}}{\text{Size of vidicon-tube raster}}$$

Since the effects of varying m_e are so closely related to the subject of raster shrinkage, detailed discussion of this subject is deferred to the section entitled "Target-Vehicle-Range Scaling and Raster Shrinkage."

The target vehicle image is formed on the face of a high-intensity projection kinescope which is capable of a maximum highlight brightness of 8000 foot-lamberts (27 410 candelas/meter^2) when the background raster is extinguished. The target image is then projected onto screen S2 by means of lens L2 and the two-gimbal mirror. The measured highlight brightness on the screen is approximately 5 foot-lamberts (17 candelas/meter^2). The two-gimbal mirror positions the target image in azimuth and elevation, which correspond to the line-of-sight (LOS) angles α and β.

Motion.- The relative rotational motion between the observer body-axis system and target-vehicle body-axis system may be broken down into two distinctly separate types as illustrated in figures 2(b) and 2(a). First, there is rotation of the LOS axis system relative to the observer body-axis system which is completely specified by the LOS angles α and β. Second, there is rotation of the target body-axis system relative to the LOS axis system which is defined by the three Euler angle rotations: ϕ_T about the $\hat{i}_2$-axis, followed by θ_T about the intermediate $\hat{j}_2'$-axis, followed by ψ_T about the $\hat{k}_3$-axis. (Note that the angles θ_T, ψ_T, and ϕ_T fully describe target aspect with respect to the LOS.) The relative rotational motions that result from basic vehicle motions are described by the following examples which are presented as an aid in visualizing these motions:

(1) Relative translation between the two vehicles results in variations of α, β, ϕ_T, θ_T, and ψ_T. However, for certain relative orientations, ϕ_T does not vary (for example, target and observer body axes parallel).

(2) Rotation of the observer vehicle results in variation of the angles α, β, and ϕ_T. However, target aspect angles $(\psi_T$ and $\theta_T)$ do not change since the axis system $\hat{i}_2,\hat{j}_2',\hat{k}_2'$ does not rotate relative to the target body-axis system $\hat{i}_3,\hat{j}_3,\hat{k}_3$.

(3) Rotation of the target body-axis system results in variations of the angles ϕ_T, θ_T, and ψ_T.

The line-of-sight angles are directly available from the main computer program so that no axis transformation is required. The transformation defining the target gimbal angles is

$$\begin{bmatrix} X_3 \\ Y_3 \\ Z_3 \end{bmatrix} = \begin{bmatrix} c\theta_T c\psi_T & c\phi_T s\psi_T + s\phi_T s\theta_T c\psi_T & s\phi_T s\psi_T - c\phi_T s\theta_T c\psi_T \\ -c\theta_T s\psi_T & c\phi_T c\psi_T - s\phi_T s\theta_T s\psi_T & s\phi_T c\psi_T + c\phi_T s\theta_T s\psi_T \\ s\theta_T & -s\phi_T c\theta_T & c\phi_T c\theta_T \end{bmatrix} \begin{bmatrix} X_2 \\ Y_2 \\ Z_2 \end{bmatrix} \tag{9}$$

Projector geometry.- Certain conditions must be satisfied in order to have the mirror drive angles α' and β' equal to the line-of-sight angles α and β. From figure 8 the following relationships may be written:

$$\tan \alpha = \frac{D'}{K + S'} \tag{10}$$

$$\tan \alpha' = \frac{D}{b} \tag{11}$$

where D' is the lateral displacement of target virtual image relative to system optic axis and D is the lateral displacement of target image on projection screen relative to system optic axis. From simple lens theory (ref. 2) the lateral magnification of the lens may be written as

$$m = \frac{D'}{D} = \frac{S'}{S} \tag{12}$$

Since $S' >> K$, equation (10) may be approximated by

$$\tan \alpha \approx \frac{D'}{S'} = \frac{D}{S} \tag{13}$$

Comparison of equations (13) and (11) indicates that if α is to equal α', then

$$b = S \tag{14}$$

which fixes the position of the mirror gimbal center relative to the screen. An identical derivation using β would show that the same requirement holds in order to have $\beta = \beta'$.

Target-Vehicle-Image Generation Equipment

Figure 9 illustrates the mechanical arrangement of the range-bed system and, in particular, the manner in which the camera assembly is mounted on the range-bed rails. A closed-loop servo system is used to position the camera assembly on the rails. Figure 10 shows a close-up view of the camera assembly, range-bed rails, and the target model mounted in the two-gimbal system. Figure 11 illustrates the relative locations of the TV projection tube, projection lens, and two-gimbal mirror. The projection-tube housing is lined with lead for protection from the X-rays generated by the 80-kilovolt projection tube. Figure 12 shows an overall view of the entire projection assembly with

the rack on the left housing the raster shrinkage equipment. The projector mounting frame is equipped with rollers for ease of movement and jack screws for vertical adjustment.

TARGET-VEHICLE RANGE SCALING AND RASTER SHRINKAGE

Derivation of Range Scaling Equations

In order to provide the full problem range excursion and still maintain correct target perspective at near range, the target-vehicle-image generation system employs a combination of physical camera motion (range bed) and projector raster shrinkage.

Correct perspective requires that the range-bed scale factor be identical with that of the target model. Therefore, the $\frac{1}{96}$-scale model fixes the maximum simulated range of the range bed at 160 meters. With this scale factor, the near limit of the range bed fixes the minimum simulated range at 10 meters. A technique has been developed which extends the maximum range capability of the system while preserving the TV image-line resolution that exists at the 160-meter range (maximum range-bed travel). This technique consists of continuously shrinking the projection-tube raster from its maximum size whenever the problem range exceeds 160 meters.

The following equation development (see fig. 13) serves to establish a relationship between model dimension and observed image dimension for the combined range bed and raster shrinkage system. The overall magnification of the television system may be determined by repeated application of the simple lens magnification equation (ref. 2) to the three lenses in figure 13, as follows:

$$\frac{J_c'}{J_c} = -\left(\frac{f_c}{r' - f_c}\right) \tag{15}$$

$$\frac{J_p}{J_c'} = m_e \tag{16}$$

$$\frac{J_p'}{J_p} = -\left(\frac{n - f_p}{f_p}\right) \tag{17}$$

$$\frac{J'}{J_p'} = -\left(\frac{S' - f_v}{f_v}\right) \tag{18}$$

Combining equations (15) to (18) results in the following equation which relates the dimension of the final image to the corresponding dimension of the target model:

$$J' = -\left(\frac{S' - f_v}{f_v}\right)\left(\frac{n - f_p}{f_p}\right)(m_e)\left(\frac{f_c}{r' - f_c}\right)J_c \tag{19}$$

The dimension J' is related to the corresponding dimension of the real-world object J by

$$\frac{J'}{S' + K} = \frac{J}{r} \tag{20}$$

Substitution of equation (20) into equation (19) results in the following expression:

$$\frac{J(S' + K)}{r} = -\left(\frac{S' - f_v}{f_v}\right)\left(\frac{n - f_p}{f_p}\right)(m_e)\left(\frac{f_c}{r' - f_c}\right)J_c \tag{21}$$

Equation (21) may be rewritten to illustrate the relationship between the range-bed range and real-world range which is used, with constant m_e, for ranges less than or equal to 160 meters. The resulting equation is

$$r' = -\left(\frac{S' - f_v}{f_v}\right)\left(\frac{n - f_p}{f_p}\right)(m_e)\left(\frac{f_c}{S' + K}\right)\left(\frac{J_c}{J}\right)r + f_c \tag{22}$$

where J_c/J is simply the model scale factor. In equation (22) the term f_c is normally small in comparison to the other term and may be neglected. Equation (21) may also be rewritten to show the relationship between the electronic magnification and real-world range which is used, with r' constant, for ranges greater than 160 meters. The resulting equation is

$$m_e = -\frac{J(S' + K)}{J_c}\left(\frac{f_v}{S' - f_v}\right)\left(\frac{f_p}{n - f_p}\right)\left(\frac{r' - f_c}{f_c}\right)\left(\frac{1}{r}\right) \tag{23}$$

General Circuit Considerations

Closed-loop computational elements are utilized to generate the desired voltage and current waveforms in a nonresonant deflection amplifier in order to provide the electronic means of symmetrically varying the size of a television raster to simulate image ranging. Figure 14 is a block diagram of a single channel of the reduction raster deflection system. A composite (horizontal and vertical) raster generator requires two similar channels. Although the deflection systems exhibit conceptual similarities in the vertical and horizontal channels, the power levels, timing, and internal gains are different. With the exception of the synchronization circuitry, the function blocks contain closed-loop chopper-stabilized computational amplifiers.

The video and synchronization voltages from the camera control are separate inputs to the projector electronics. The projector electronics consist of a high-gain video amplifier and a specially designed sweep-drive unit. The sweep-drive unit is designed so that the size of the projection-tube raster may be varied continuously under control of the main program range signal. Since only the size of the raster is being varied, the number of raster lines contained in the image is constant. As the raster size is reduced,

the tube beam current must be reduced proportionately to maintain constant image brightness. This action also prevents damage to the tube phosphor, especially at small raster sizes.

Deflection Circuitry

The deflection amplifier is a classical feedback circuit which converts the sum of the input voltage waveforms to a proportional yoke current waveform. The conversion accuracy is dependent upon the deflection driver's open-loop gain-bandwidth response. The voltage excursion capability is governed by the rapid retrace speed of the sawtooth current passing through the inductive yoke element.

Full raster size corresponds to a half-axis deflection angle of 11^{o} with deflection angle being linearly proportional to deflection current. Image brightness considerations require a cathode-ray-tube ultor voltage of 80 kilovolts. The horizontal deflection current for a 10-microhenry deflection coil is 10 amperes (full-size raster).

The deflection amplifier is driven by two signals: a voltage sawtooth and a negative dc bias both of which are proportional to the range input voltage. A yoke current waveform, symmetrical about a zero reference, will be generated if the magnitude of the bias offset is equal to one-half the magnitude of the sawtooth voltage. Variation of the range input voltage will cause a symmetrical variation of the yoke current, and hence of the raster, about a zero-current center. In addition to satisfying the feedback requirements of the deflection amplifier, the voltage waveform obtained at the current sensing resistor provides the intensity control circuitry with a reference voltage that is directly proportional to the raster size.

The analog range input and the synchronization pulses are buffered for noise. A common mode rejection circuit is used for the analog input and contains an inverter-amplifier configuration which subtracts the common mode voltage from the analog computer input. In addition, this circuit provides low impedance drive ahead of the voltage stages of the raster generator. The signal conditioning circuitry provides a 2.5-volt noise rejection threshold for incoming synchronization pulses.

Figure 15 illustrates the circuit configuration of the high-speed, resettable, bootstrap integrator used to generate the voltage sawtooth sweeps. The integrator is formed by a feedback arrangement of two inverting amplifiers. Linear voltage ramps are generated by a constant-current charging capacitor C1. Transistor Q1 operates as a switch and provides the discharge current path for capacitor C1 during retrace time intervals. Synchronization pulses applied to the base of Q1 define sweep and reset times.

The following derivation assumes A1 and A2 to be ideal computational amplifiers. A current summation at node A for Q1 in a nonconducting state yields

$$I_2 = I_3 - I_1$$

or

$$I_2 = \frac{(E_2 - E_c)}{R_6} - \frac{E_c}{R_1} \tag{24}$$

With

$$E_2 = \frac{-R_5 E_1}{R_3} - \frac{R_5 E_r}{R_4}$$

and

$$E_c = -\frac{R_1 E_1}{R_2}$$

equation (24) takes the form

$$I_2 = -\frac{R_5 E_1}{R_6 R_3} - \frac{R_5}{R_4 R_6} E_r + \frac{R_1}{R_2 R_6} E_1 + \frac{E_1}{R_2} = -\frac{R_5}{R_4 R_6} E_r + E_1 \left(\frac{R_6 + R_1}{R_2 R_6} - \frac{R_5}{R_3 R_6} \right) \tag{25}$$

If

$$\frac{R_5}{R_3} = \frac{R_6 + R_1}{R_2} \tag{26}$$

equation (25) reduces to

$$I_2 = -\frac{R_5}{R_4 R_6} E_r \tag{27}$$

The current I_2 may also be expressed as

$$I_2 = C_1 \frac{dE_c}{dt} = -\frac{C_1 R_1}{R_2} \frac{dE_1}{dt} \tag{28}$$

Substituting equation (28) into equation (27) results in

$$\frac{dE_1}{dt} = \frac{R_2 R_5 E_r}{R_1 R_4 R_6 C_1}$$

or

$$E_o = \frac{R_2 R_5}{R_1 R_4 R_6 C_1} \int E_r \, dt \tag{29}$$

Equation (29) defines the output E_1 to be a linear voltage ramp for the condition of a dc input reference voltage. Ramp linearity is dependent upon the practical realization of resistive equality as defined by equation (26), inequality resulting in either a bow or sag in ramp voltage. The most stringent requirement which the practical circuit

places upon the ideal configuration is that of bandwidth. The problem is minimized, however, in that the amplifiers operate with a near unity-gain feedback loop. The reset speed achieved by the horizontal sawtooth generator is of the order of 1 microsecond. The feedback integrator afforded a method of referencing the chopper transistor Q1 to a circuit ground rather than the virtual ground of an operational amplifier summing junction.

The transfer characteristics of the deflection amplifier are derived for the amplifier configuration of figure 16. The derivation assumes one input voltage. Node B is a summing junction and performs the arithmetic sums of multiple inputs. This fact is later used to establish the operating point of the sweep amplifier.

The input signal is amplified and applied to the yoke and sensing resistor combination (L and R_9). The yoke current waveform obtained at node C is returned to node B by the resistance path R8. The subtraction process reduces to zero the arithmetic difference between the applied current waveform and the yoke current waveform.

If the input impedance of amplifier A3 is high and if $R_9 \ll R_8$, then the voltage present at node B can be expressed as

$$E_B = \frac{(E_{in} - I_4 R_9) R_8}{R_7 + R_8} + I_4 R_9 \tag{30}$$

The open-loop gain of amplifier A3 is defined to be $-\mu$; therefore,

$$-\frac{E_3}{\mu} = \left[\frac{(E_{in} - I_4 R_9) R_8}{R_7 + R_8} + I_4 R_9\right] \tag{31}$$

If the open-loop gain of the amplifier is large, then from equation (31)

$$I_4\left(R_9 - \frac{R_8 R_9}{R_7 + R_8}\right) = \frac{-R_8 E_{in}}{R_7 + R_8}$$

Reducing this equation gives

$$I_4 = \frac{-R_8 E_{in}}{R_7 R_9} \tag{32}$$

Equation (32) defines a linear relationship between the output current and the input voltage if the gain of the amplifier is large. Equations (29) and (32), in conjunction with yoke test data, are used to establish the voltage and current deflection parameters. The gain of the bias amplifier (fig. 17) establishes a current offset equal to one-half of the sweep current.

Figure 17 illustrates the basic dc circuit for the horizontal and vertical deflection amplifiers. The power stage, shown in transistor form, contains a number of current stages which are represented by Q3 and Q4. Resistors R10 and R11 compensate for unequal current gains in addition to providing circuit stability. The amplifier is biased by diode D1 to permit a controlled amount of current to pass from transistor Q3 to Q4. This action minimizes the crossover distortion that is present at ground level. Resistor R8 defines the feedback path for both the voltage and current waveforms obtained at R9. The power amplifier is driven by a high bandwidth voltage amplifier denoted by A3.

The dc voltage gain of the power amplifier approaches that of a complementary emitter follower. The transient response, however, is somewhat less than a complementary pair owing to the increased capacitance introduced by the large surface area of the heat sinks which were directly connected to the collector to achieve the necessary heat dissipation.

In order to maintain a constant picture brightness, with respect to a varying raster size, it is necessary to modulate the intensity of the projection tube with an appropriate variable bias voltage. Figure 18 depicts the intensity control circuitry. The vertical and horizontal sweep currents are sensed and the summation of these terms is functionally coupled to the control grid of the cathode-ray tube. It is necessary to provide a vertical retrace blanking period to overcome the transient capability of the vertical amplifiers; that is, less than 50 microseconds of the available 0.5 millisecond are needed for current retrace. By serrating this dc bias voltage with the vertical retrace pulse, it is possible not only to provide the required vertical blanking but also to allow capacitive coupling of the resulting waveform into the control grid of the cathode-ray tube. Diode dc restoration inhibits the cumulative waveform sag. Amplifier A4 provides the necessary voltage gain for the unblank pulse, and the threshold supply determines the initial projection-tube bias.

EULER ANGLE COMPUTERS

The gimbal angles for the different projectors are provided to the simulator in the form of direction cosine matrices, the matrix elements being generated by means of the quaternion rate equations (ref. 3). In this section is discussed the mechanization of the special-purpose computers which convert the matrix elements into the required shaft angles.

The transformation matrix for each set of gimbals has been defined previously in this report. For all gimbals the order of rotation is roll ϕ, pitch θ, and yaw ψ. The general form of this matrix is repeated to illustrate the trigonometric dependence of each matrix element upon the gimbal angles as follows:

$$\begin{bmatrix} X \\ Y \\ Z \end{bmatrix}_{\text{rotating}} = \begin{bmatrix} (c\theta_1 c\psi_1) & (c\phi_1 s\psi_1 + s\phi_1 s\theta_1 c\psi_1) & (s\phi_1 s\psi_1 - c\phi_1 s\theta_1 c\psi_1) \\ (-c\theta_1 s\psi_1) & (c\phi_1 c\psi_1 - s\phi_1 s\theta_1 s\psi_1) & (s\phi_1 c\psi_1 + c\phi_1 s\theta_1 s\psi_1) \\ s\theta_1 & -s\phi_1 c\theta_1 & c\phi_1 c\theta_1 \end{bmatrix} \begin{bmatrix} X \\ Y \\ Z \end{bmatrix}_{\text{fixed}} \tag{33}$$

where subscript 1 refers to the resolver input and subscript 2 refers to the actual resolver shaft position in figure 19. For an arbitrary relative orientation between the axis systems, the transformation matrix of equation (33) takes on the following form of a matrix of nine direction cosines:

$$\begin{bmatrix} X \\ Y \\ Z \end{bmatrix}_{\text{rotating}} = \begin{bmatrix} a_{11} & a_{12} & a_{13} \\ a_{21} & a_{22} & a_{23} \\ a_{31} & a_{32} & a_{33} \end{bmatrix} \begin{bmatrix} X \\ Y \\ Z \end{bmatrix}_{\text{fixed}} \tag{34}$$

where the a_{ij}'s represent the direction cosines between respective axes in the two systems. In particular, the direction cosines which define the axis transformations referred to in figure 3 are specified by the elements b_{ij}, c_{ij}, and d_{ij}. In equations (33) and (34) the same convention of transformation from a fixed axis system to a rotating axis system has been maintained.

If the definition of the fixed and rotating axis systems is identical for the simulator and computer mathematical model, then the a_{ij}'s in equation (34) are identical with the respective matrix elements in the mathematical model. If, however, the mathematical model definition of fixed and rotating axis systems is opposite to that of the simulator, then the a_{ij}'s in equation (34) must be set equal to the elements of the inverse (transpose) mathematical model matrix.

Two noteworthy characteristics of the matrix elements are as follows:

(1) The value of each a_{ij} is always between +1.0 and -1.0 which simplifies amplitude scaling of the analog computer.

(2) There is no specific order of rotation implied in equation (34) which means that the same input matrix may be used to represent simultaneously any or all six possible orders of rotation for a three-gimbal system.

Figure 19 shows the mechanization of an Euler angle computer for the order of rotation $(\phi_1, \theta_1, \psi_1)$. Each level of computation labeled "A" to "E" is made up of a polar resolver (ref. 4) utilizing the mechanization convention illustrated in the lower right-hand corner of the figure. Equation (33) shows that the elements of row three of the matrix contain sufficient information to determine the two angles ϕ_1 and θ_1. However, it

must be noted that the angle ϕ_1 is not properly defined at $\theta_1 = 90^o$. This situation corresponds to gimbal lock and is described in a subsequent paragraph.

The elements a_{32} and a_{33} are applied as inputs to the A level of computation; this results in the two outputs shown in figure 19. The output of line 1 provides the null signal $\left[\cos \theta_1(0)\right]$ to drive the ϕ_2 servo. Output 2 consists of $\cos \theta_1$ which combined with $a_{31} = \sin \theta_1$ forms the inputs to the B level of computation. The outputs of level B are defined by the convention used for level A. To compute the yaw angle ψ_1, the terms $\cos \psi_1$ and $\sin \psi_1$ must be isolated from among the remaining six terms of the matrix. Although elements a_{11} and a_{12} seem to be the most obvious choice, use of these two elements would introduce an undefined point in ψ_1 identical to that which occurs in the ϕ_2 computation. An alternate solution to the problem is to perform the algebraic operations on the second row indicated in the D and E levels of computation. (The first row of equation (33) would also satisfy this requirement and the choice of either one is arbitrary.) The result of these operations provides the two inputs $\left(\sin \psi_1 \text{ and } \cos \psi_1\right)$ to the C level of computation, the operation of which is identical to the operation of the A and B levels. Sign inversions of signals are used where indicated so that the same convention may be utilized in all levels of computation.

Even though the matrix elements exhibit no discontinuities, the Euler angle computer does encounter an indeterminate point at $\theta_1 = \pm 90^o$. This condition corresponds to the normal gimbal lock condition of a three-gimbal system and may be seen in figure 19 by observing that the null signal for the ϕ_2 servo is multiplied by $\cos \theta_1$. Thus, as θ_1 approaches $\pm 90^o$, the voltage gradient of the null signal decreases. This is the normal situation for a polar resolver and the common remedy is to vary the servo gain inversely with $\cos \theta$. However, as the $\theta = 90^o$ point is reached, the automatic gain control is no longer effective in maintaining servo position. At this point the ϕ_2 shaft may drift away from its last known value. The drift of the ϕ_2 shaft is compensated for by an equal and opposite motion of the ψ_2 shaft since ψ_2 and ϕ_2 are coupled together through the C and D levels of computation. Any drift which is introduced as herein described is automatically eliminated as soon as the system emerges from gimbal lock because the ϕ_2 shaft once again is providing the correct solution.

The mechanization described provides a solution which is piecewise continuous. When the singularity is encountered, either of two solutions may result upon emerging from the singularity. Therefore, if the system must pass in the vicinity of $\theta = \pm 90^o$, to provide predictable behavior it becomes desirable to include logic which restricts the solution to only one of the two possible solutions.

CONCLUDING REMARKS

A screen-type-refractive-virtual-image simulator has been designed and built at the Langley Research Center and has been applied to space rendezvous simulation for the Gemini program. Its applications have been extended to research in general visual techniques which will be pertinent to future space-flight activities.

A brief description has been presented of the more prominent features of the simulator equipment, two of which are worthy of mention. First, a method of continuously shrinking the raster on an 80-kilovolt kinescope projector provides the simulator with an extended range capability and still maintains target-vehicle-image line resolution. Second, the use of direction cosines to define the axis transformations and of Euler angle computers to derive the gimbal angles from elements of these matrices has provided the system with complete fly-around capability. This simulator has received a high degree of pilot acceptance which is due largely to the virtual-image display and the fly-around capability.

Langley Research Center,
National Aeronautics and Space Administration,
Langley Station, Hampton, Va., December 18, 1968,
125-19-06-01-23.

REFERENCES

1. Goldstein, Herbert: Classical Mechanics. Addison-Wesley Pub. Co., Inc., c.1959.

2. Jenkins, Francis A.; and White, Harvey E.: Fundamentals of Optics. Third ed., McGraw-Hill Book Co., Inc., 1957.

3. Robinson, Alfred C.: On the Use of Quaternions in Simulation of Rigid-Body Motion. WADC Tech. Rep. 58-17, U.S. Air Force, Dec. 1958. (Available from DDC as AD No. 234422.)

4. Rogers, A. E.; and Connolly, T. W.: Analog Computation in Engineering Design. McGraw-Hill Book Co., Inc., 1960.

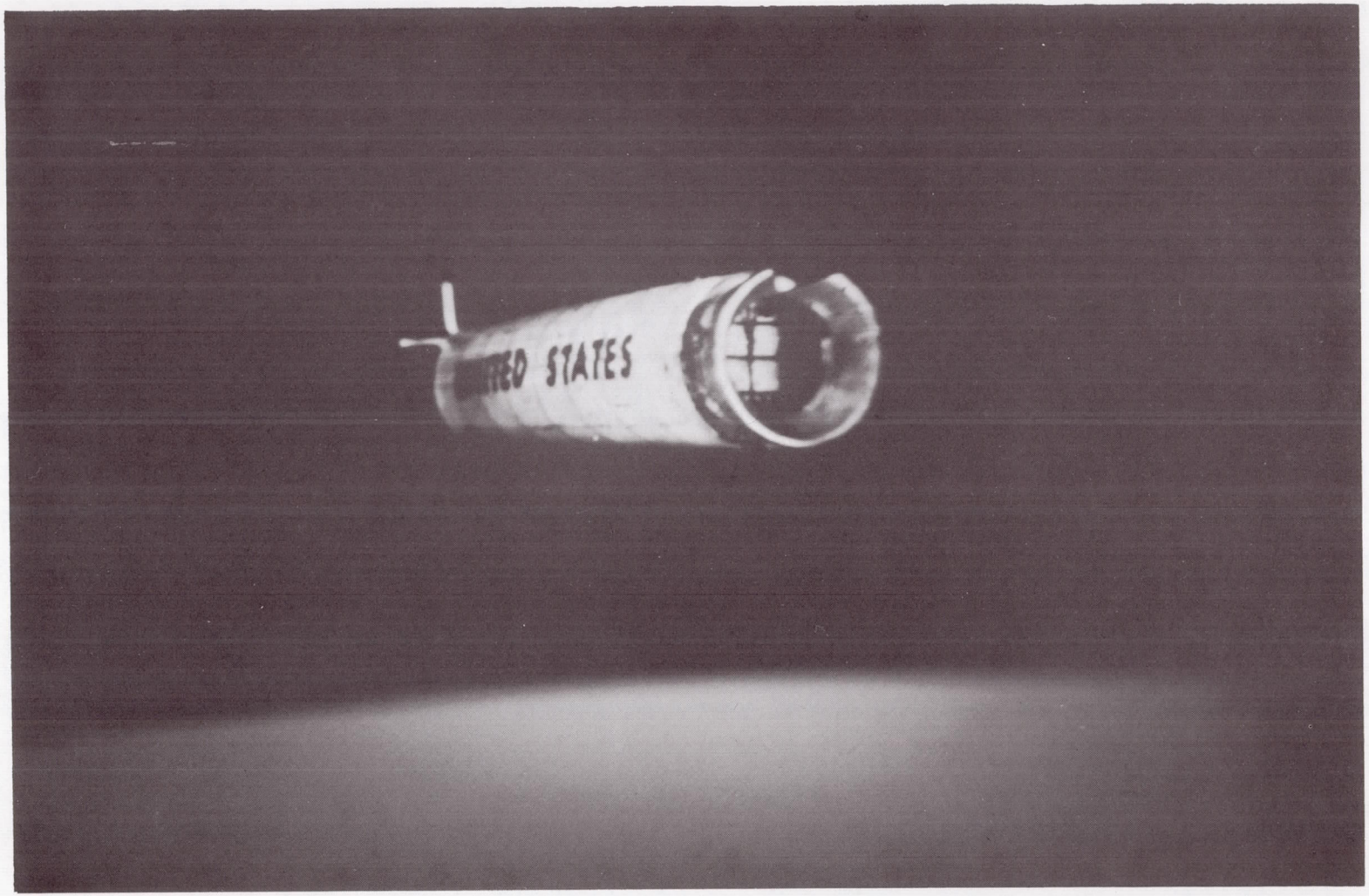

Figure 1.- Combined target and horizon images. L-66-3296

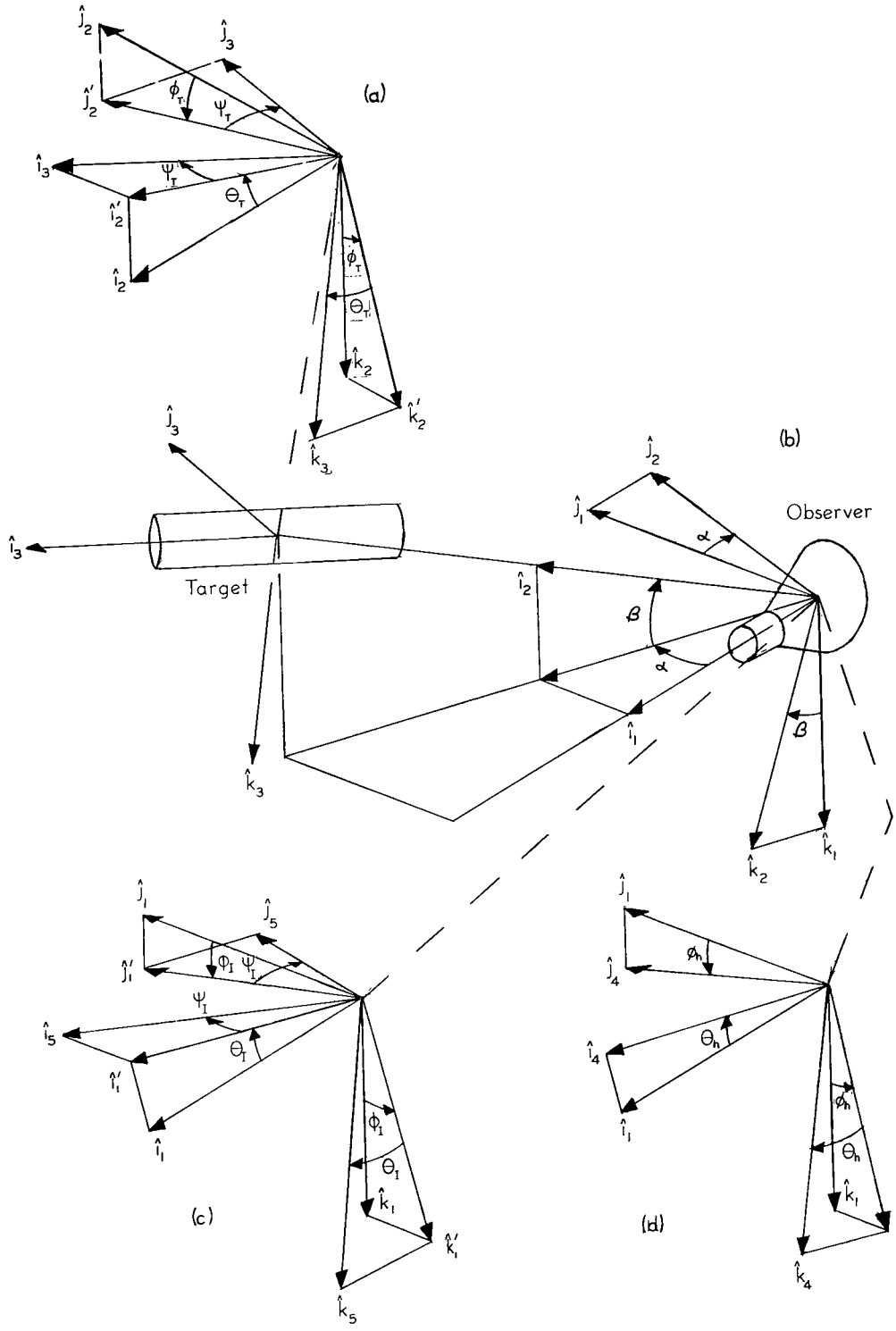

Figure 2.- System relative geometry.

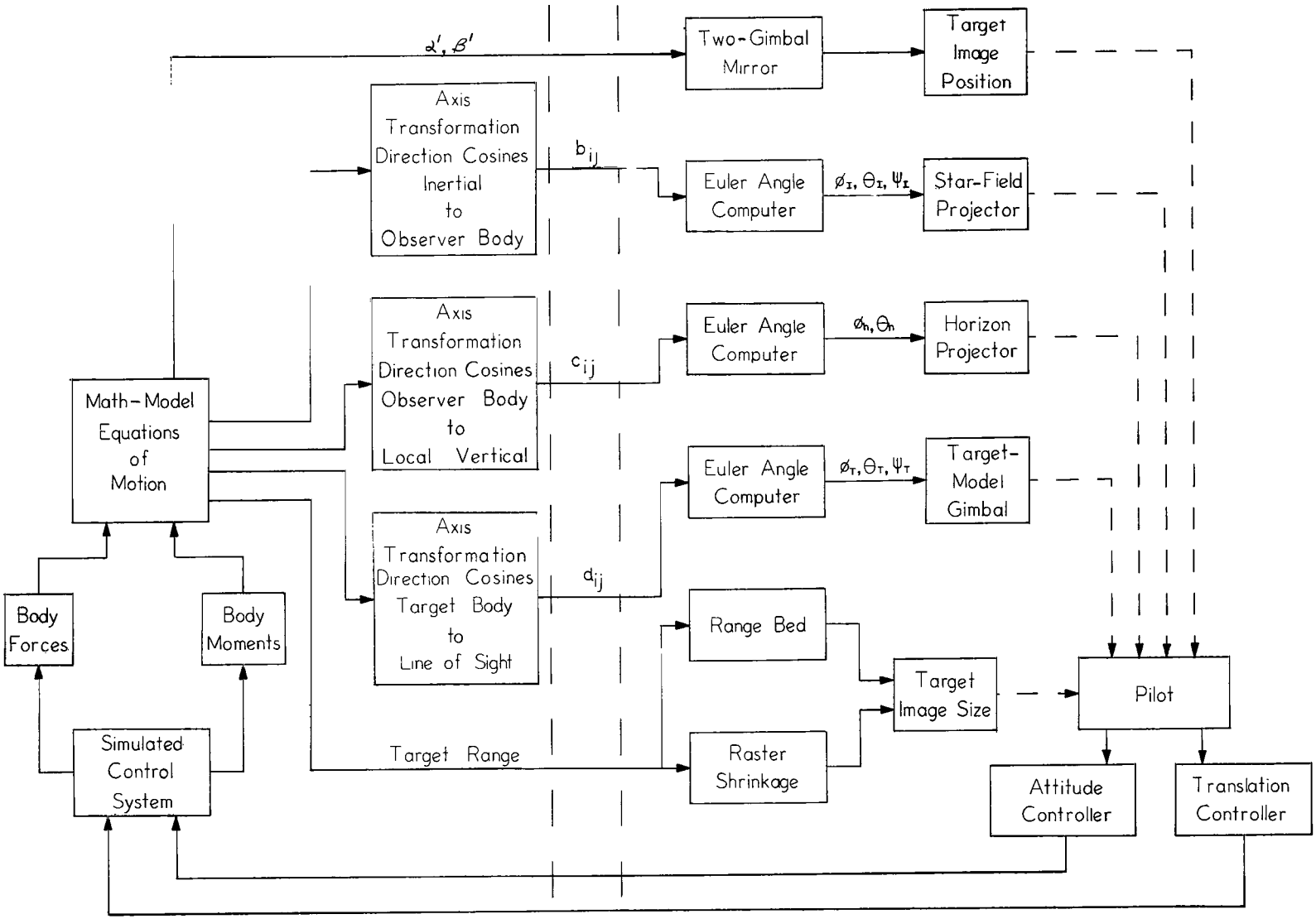

Figure 3.- Block diagram of simulator system.

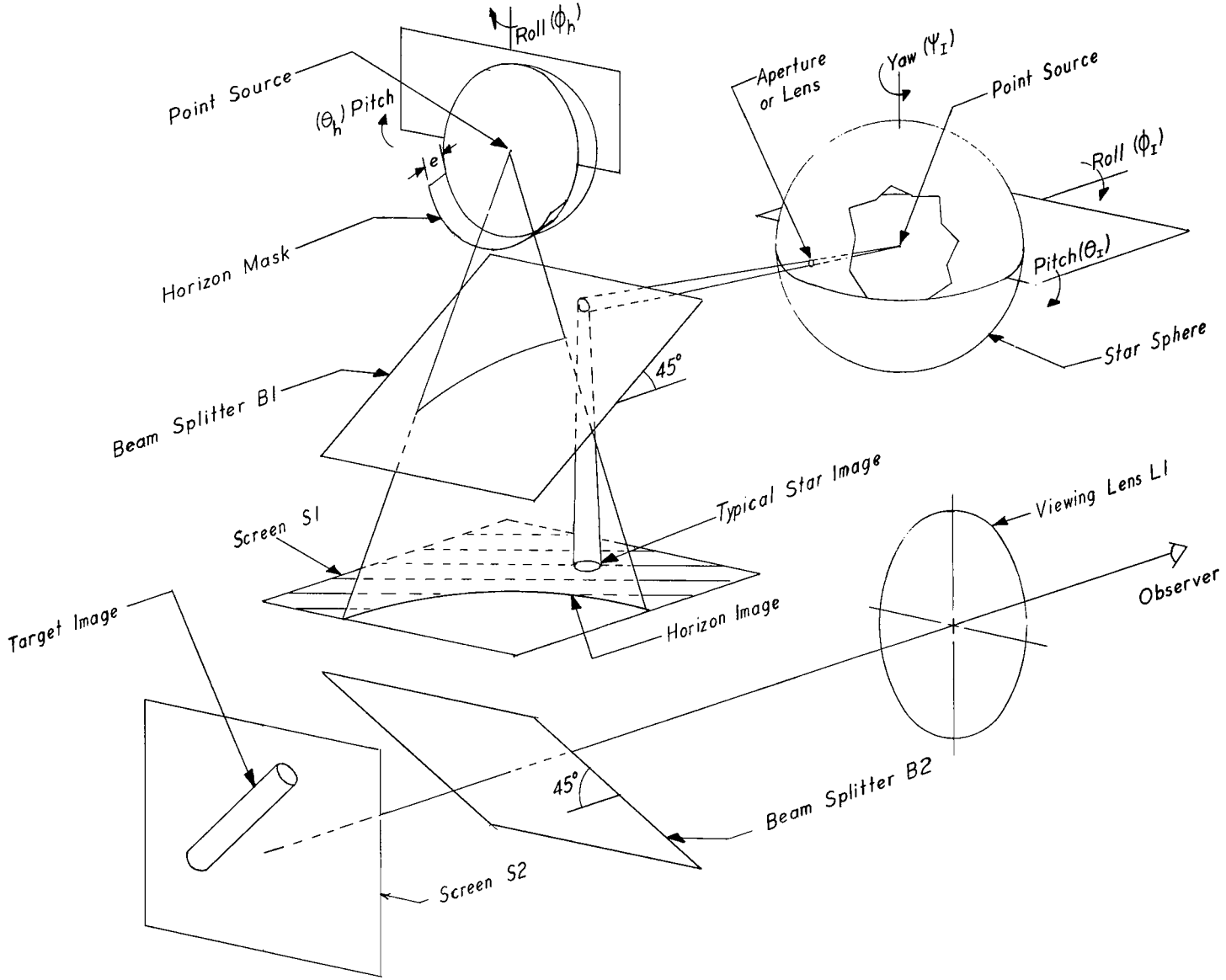

Figure 4.- Projection and combination of the star-field, horizon, and target images.

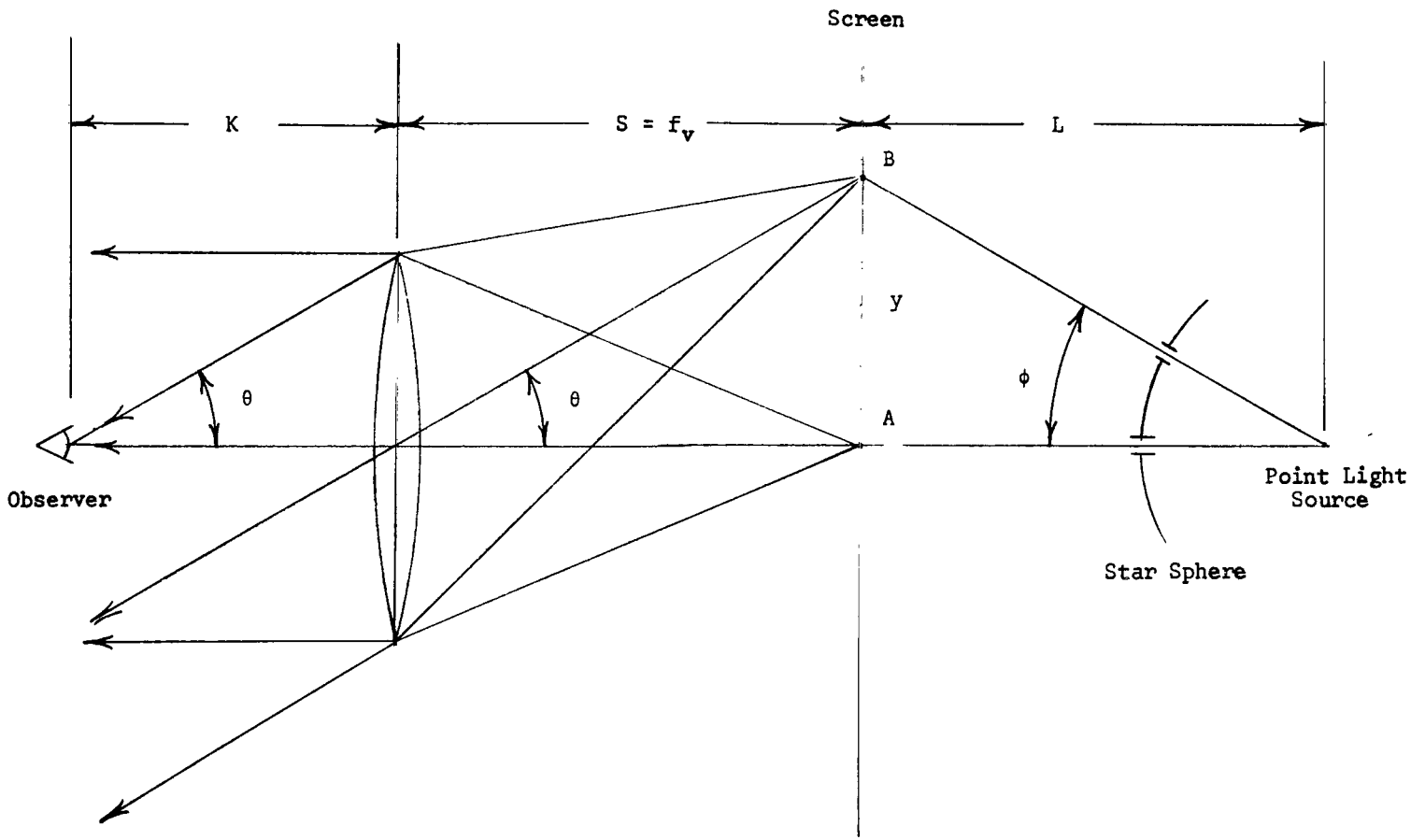

Figure 5.- Angular relationships between observer and projector when scene is viewed as a virtual image at infinity.

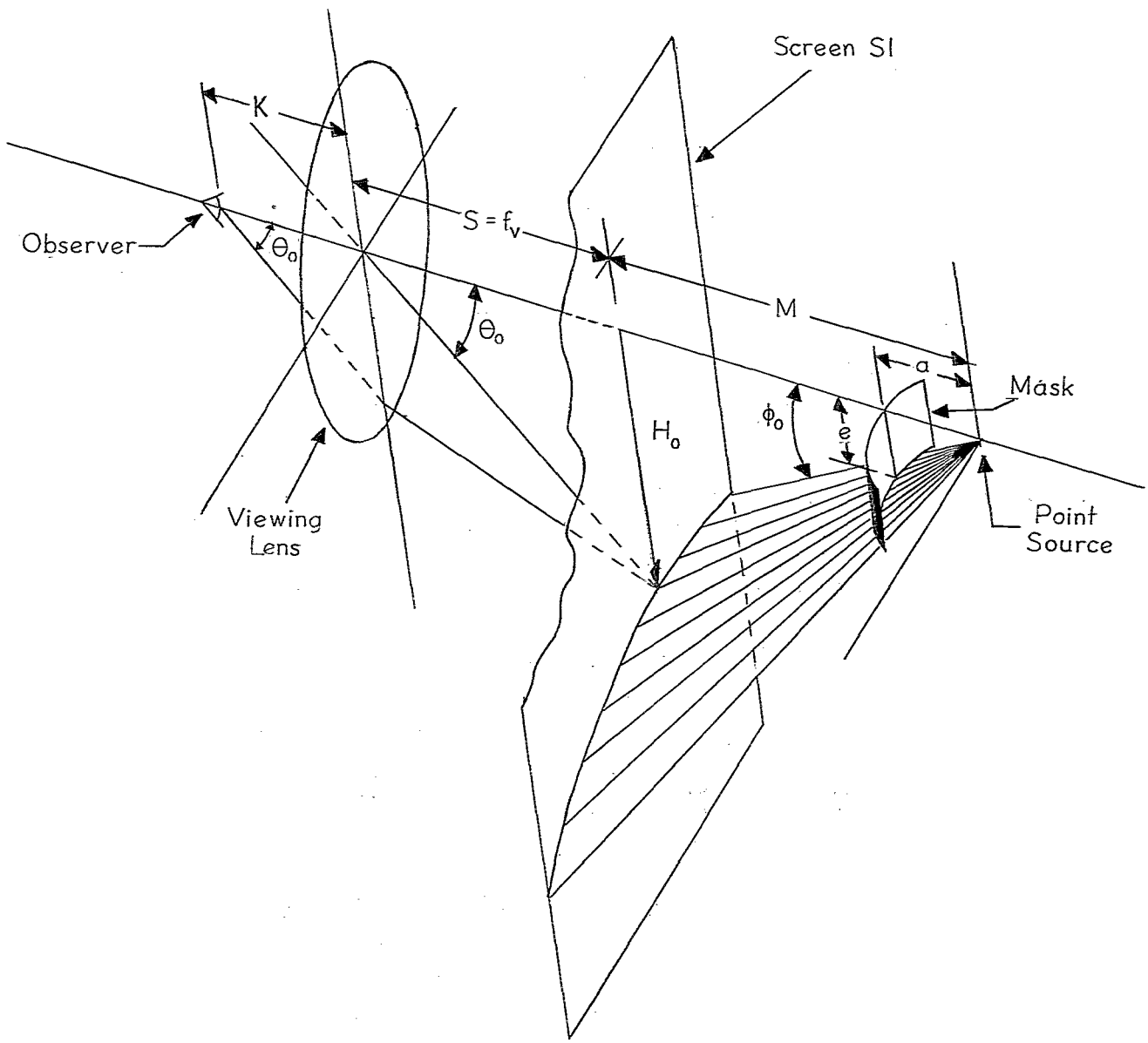

Figure 6.- Relationship between horizon mask height and horizon depression angle.

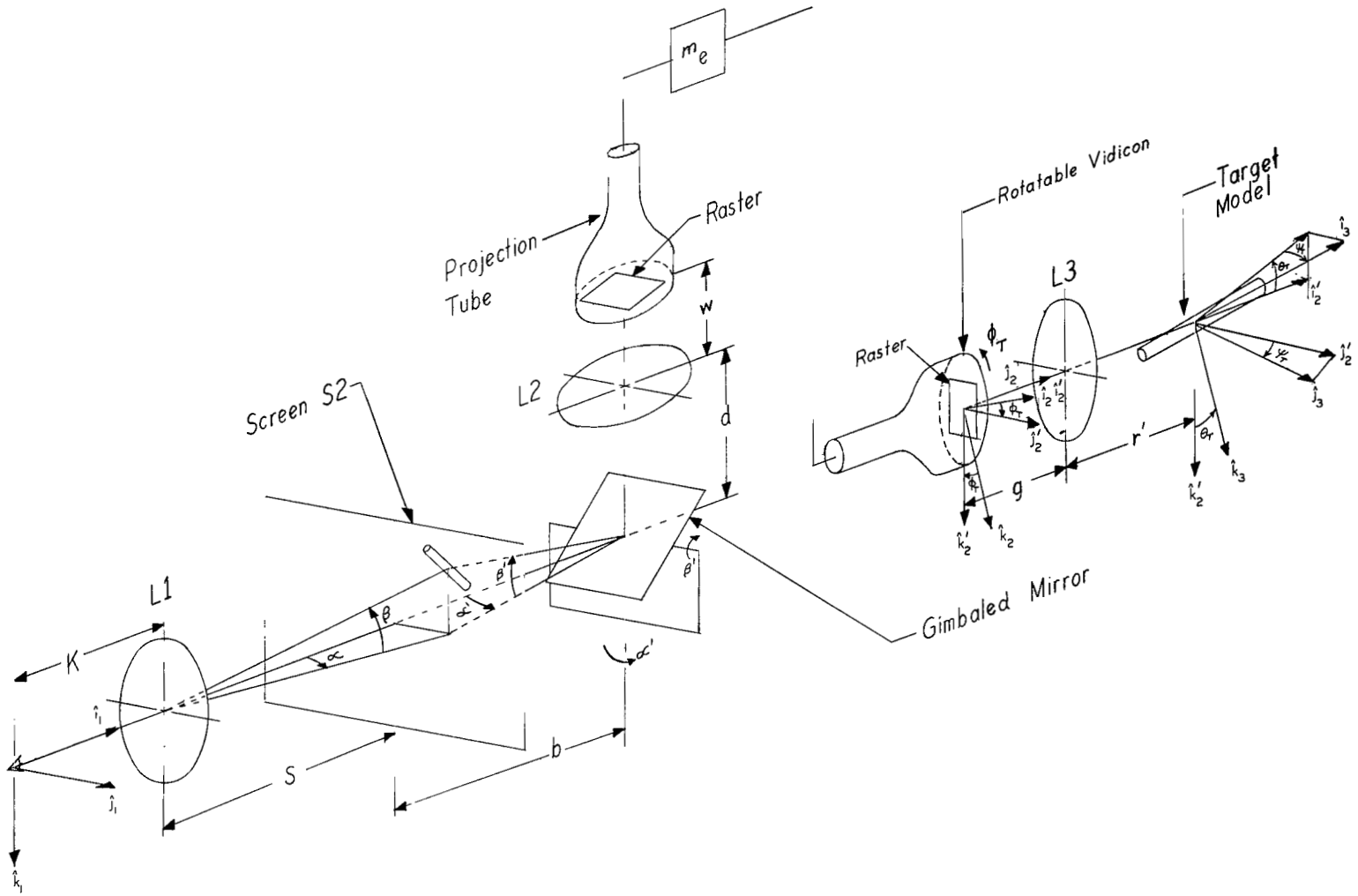

Figure 7.- Target-image generation and projection.

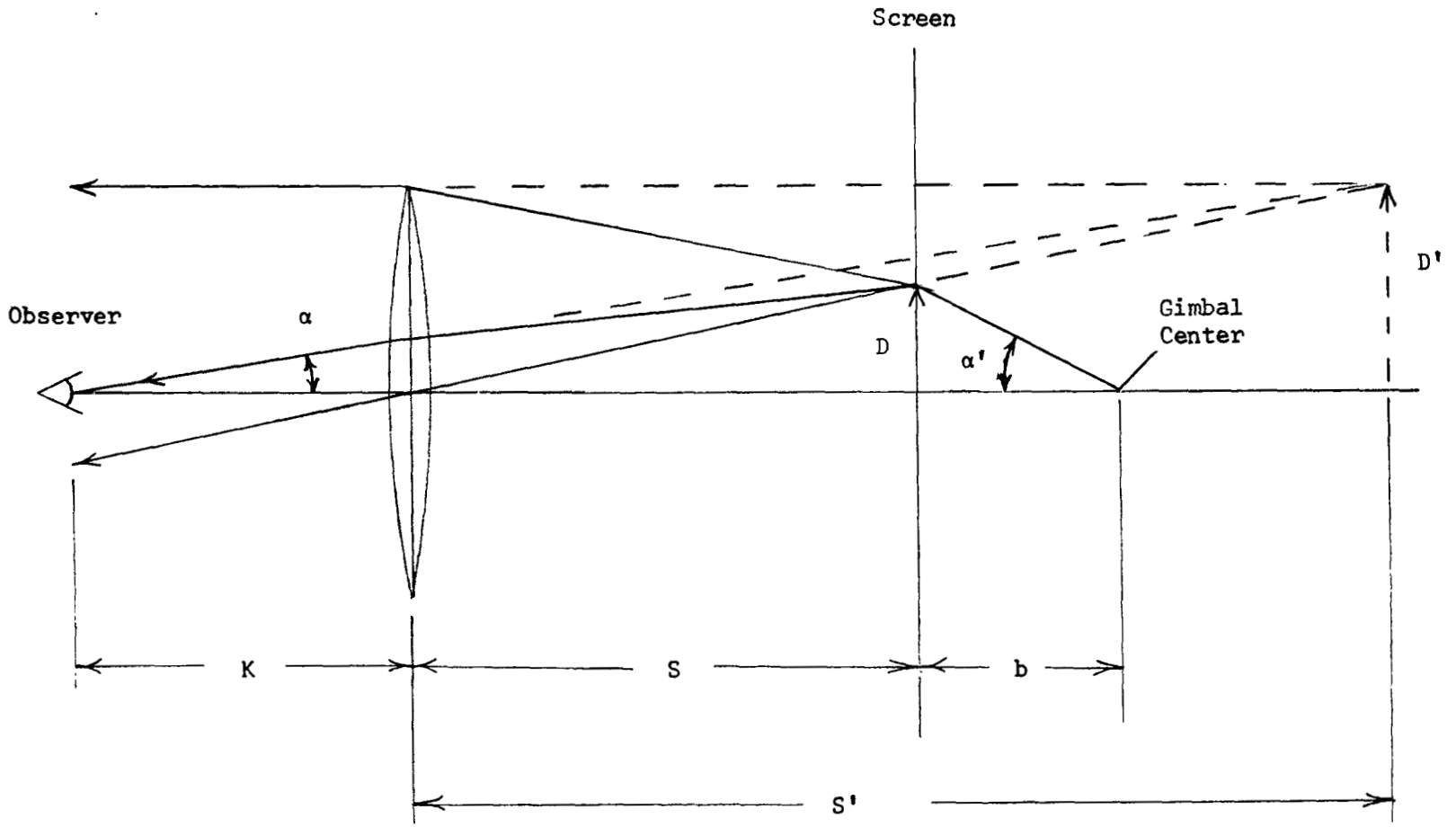

Figure 8.- Illustration of the dependence of mirror angle scaling on the projection distance.

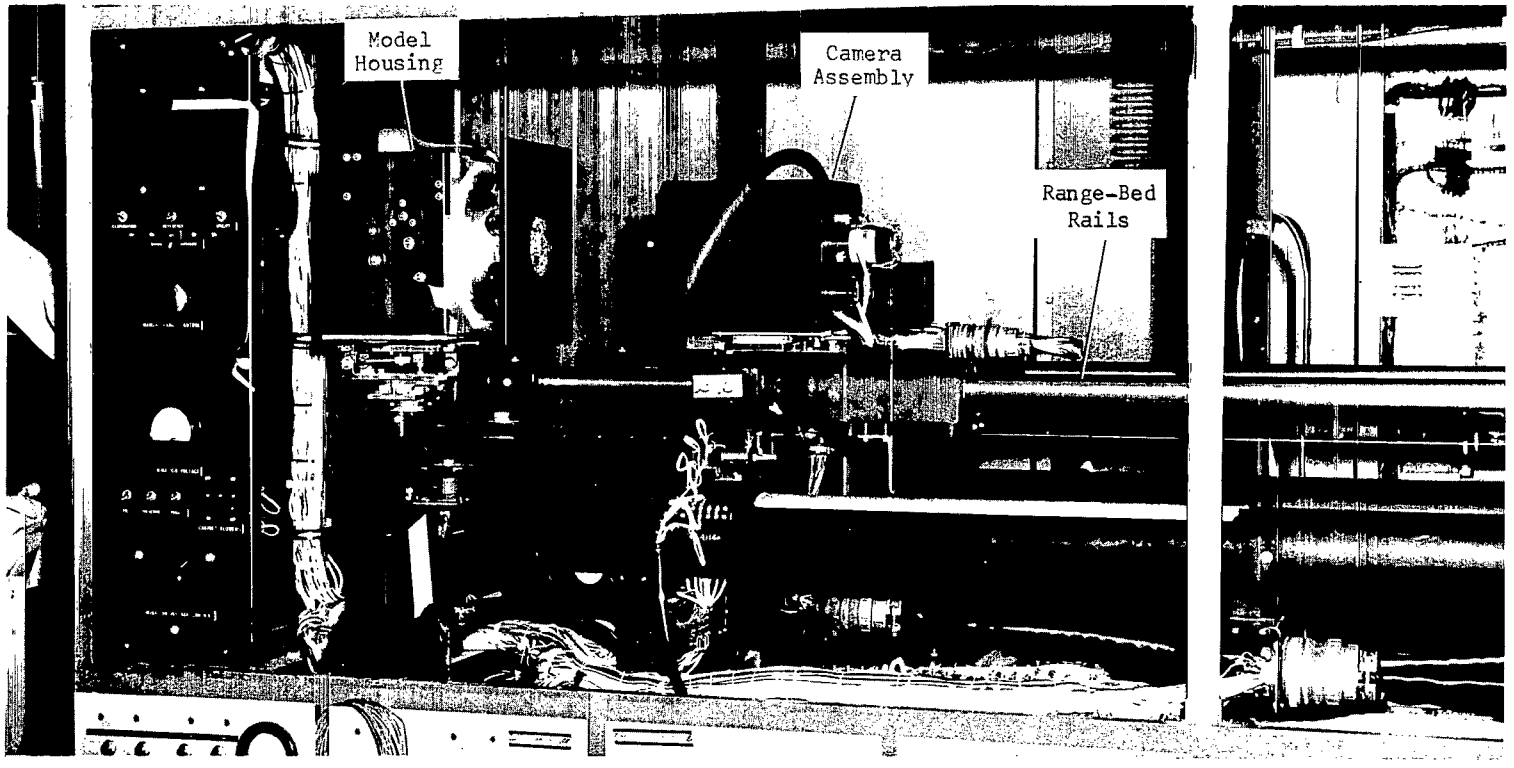

Figure 9.- Range bed.

L-66-1636.1

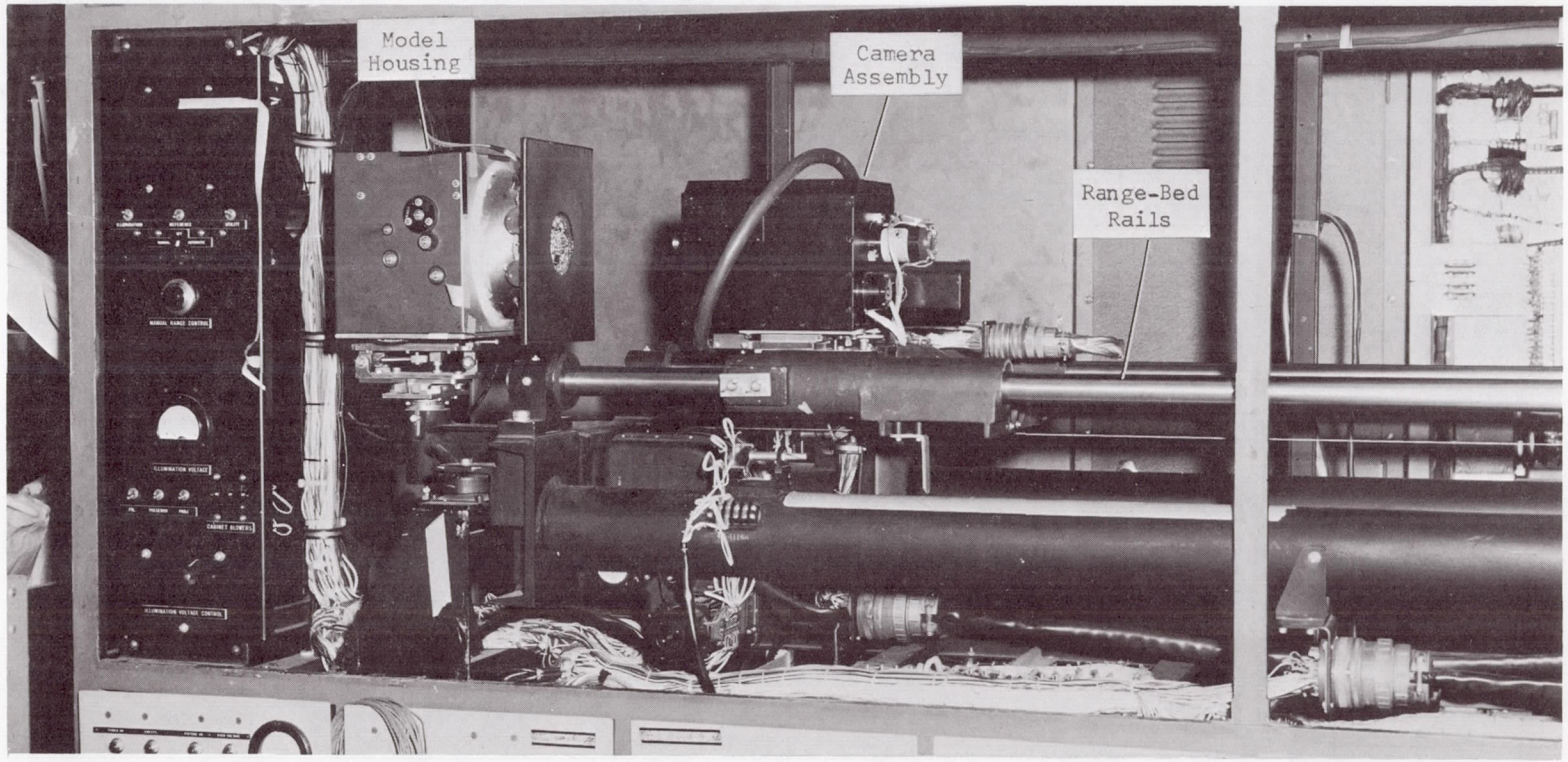

Figure 9.- Range bed.

L-66-1636.1

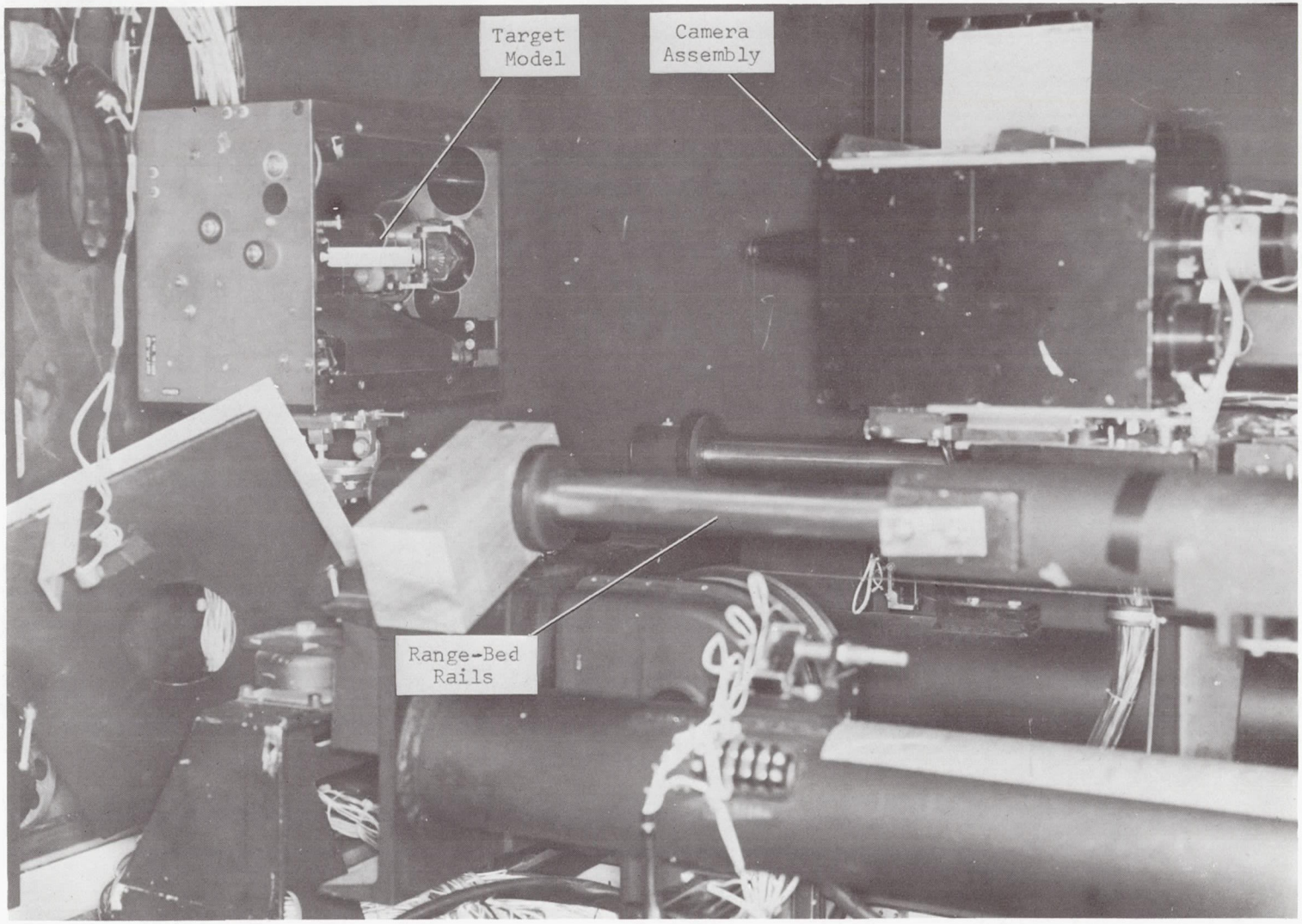

Figure 10.- Gimbaled target model and camera assembly.

L-66-5848.1

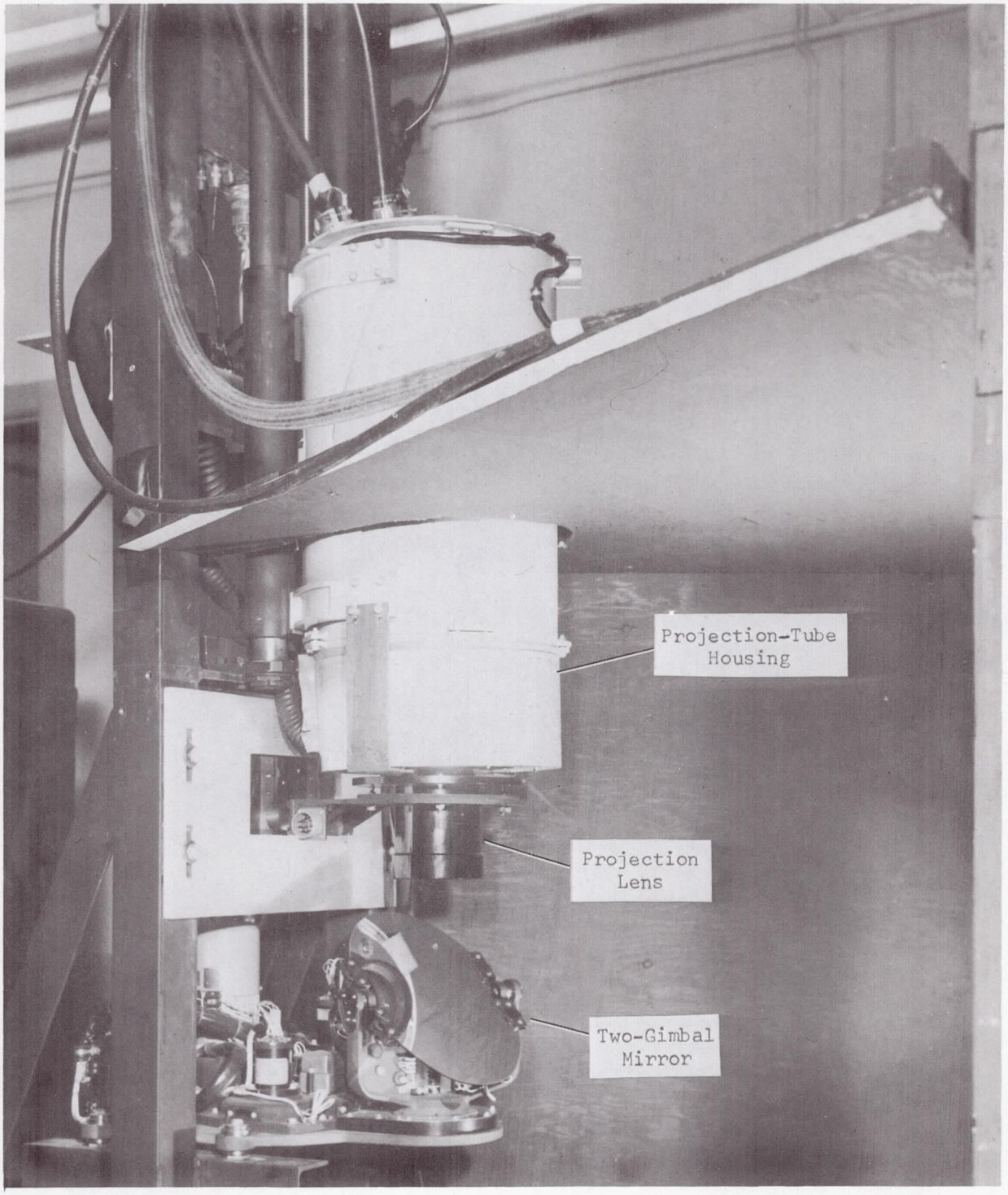

Figure 11.- TV projector showing the projection lens and two-gimbal mirror. L-66-5849.1

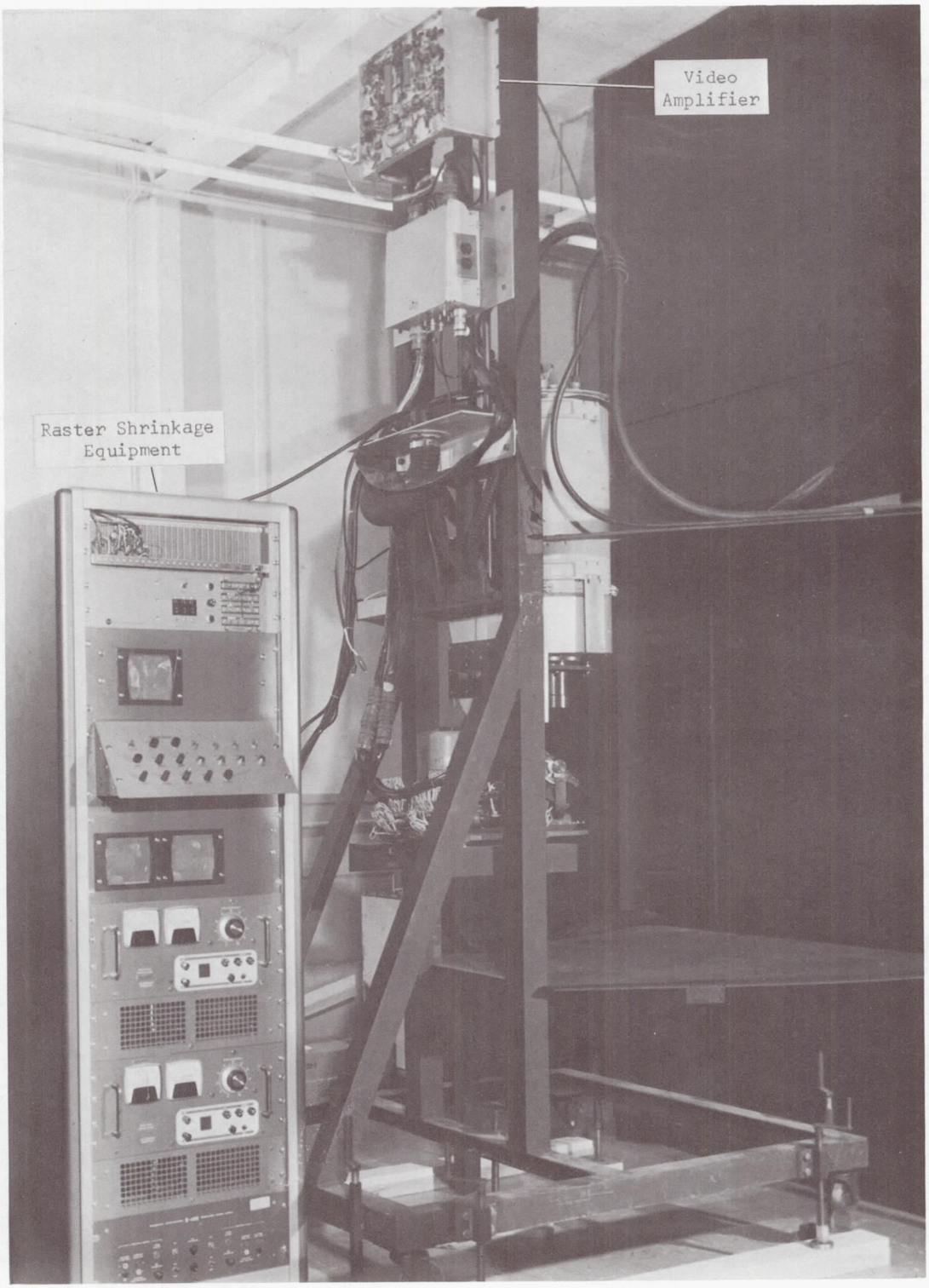

Figure 12.- TV projector and raster control unit. L-66-5850.1

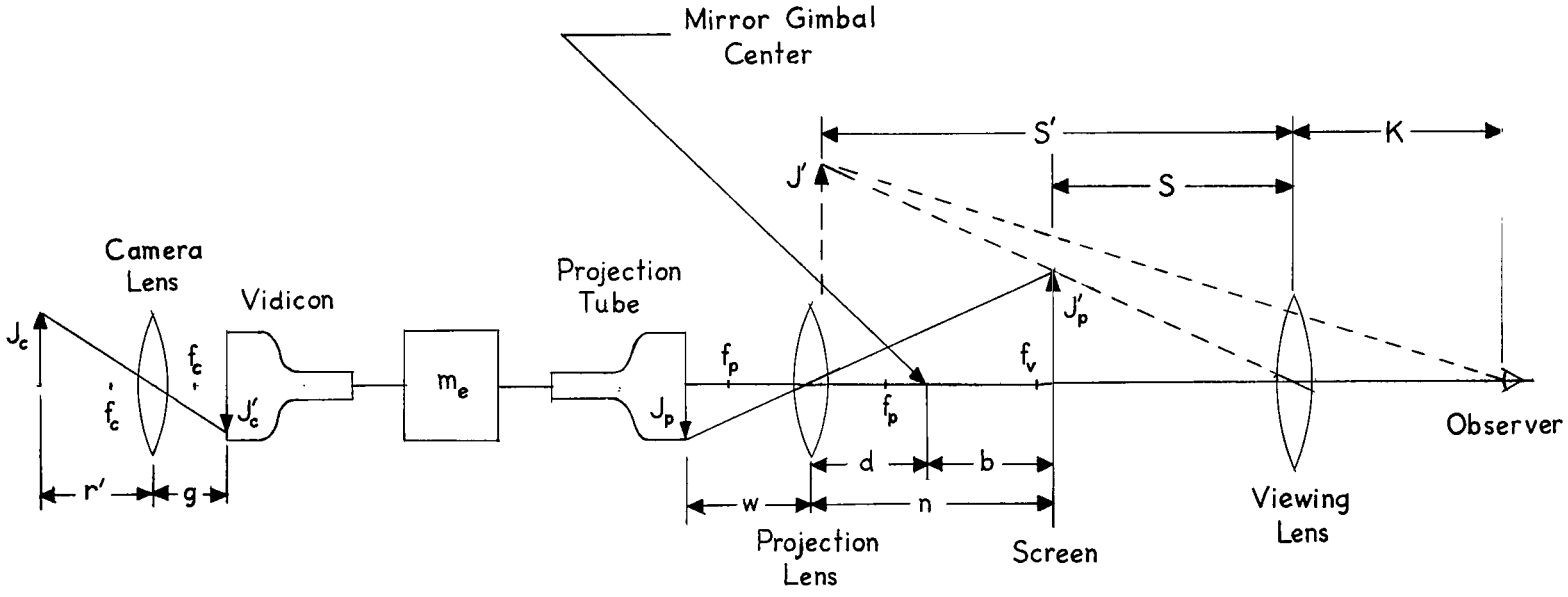

Figure 13.- Relationship between target image size and target range.

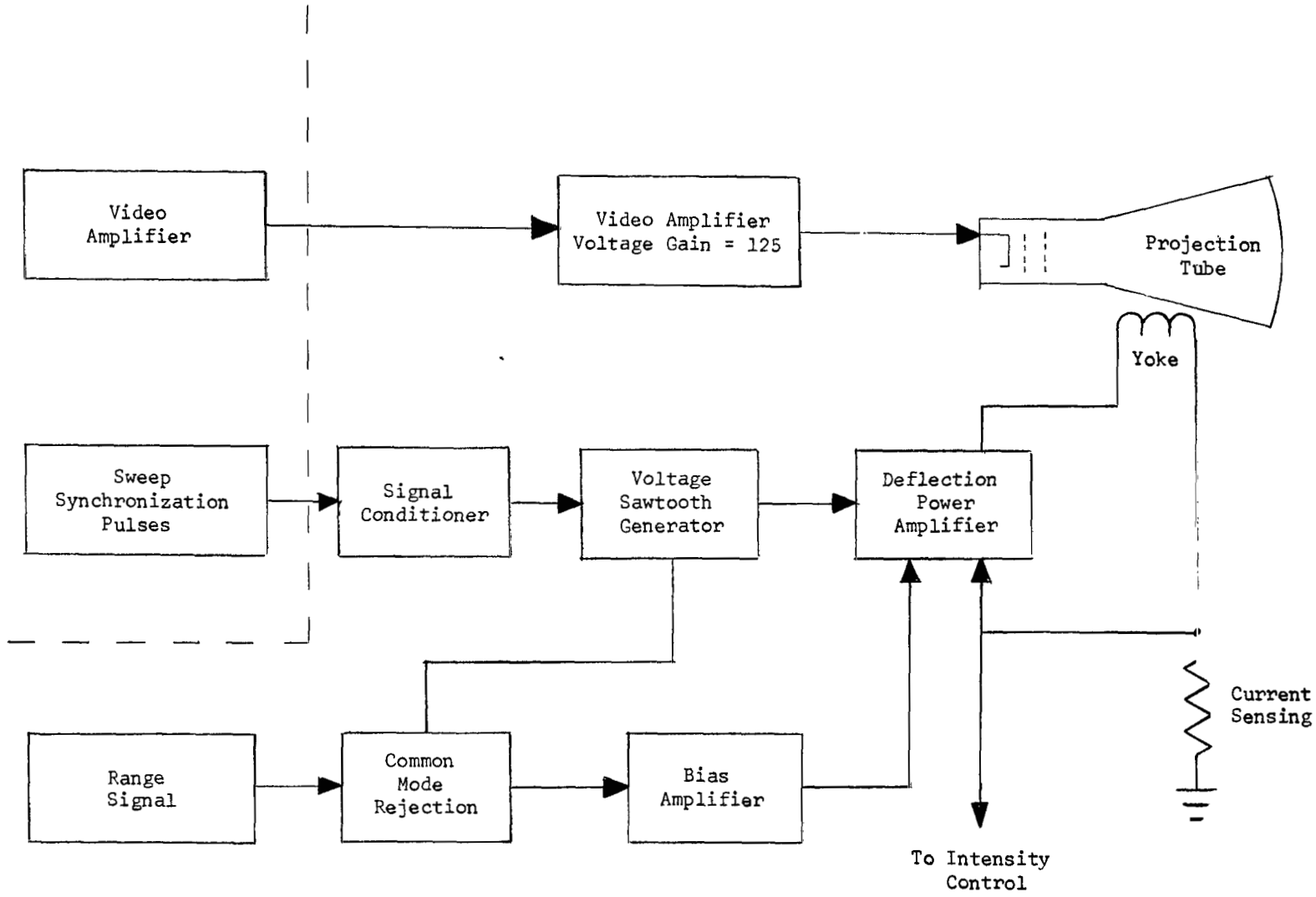

Figure 14.- Function block diagram of the projector electronics.

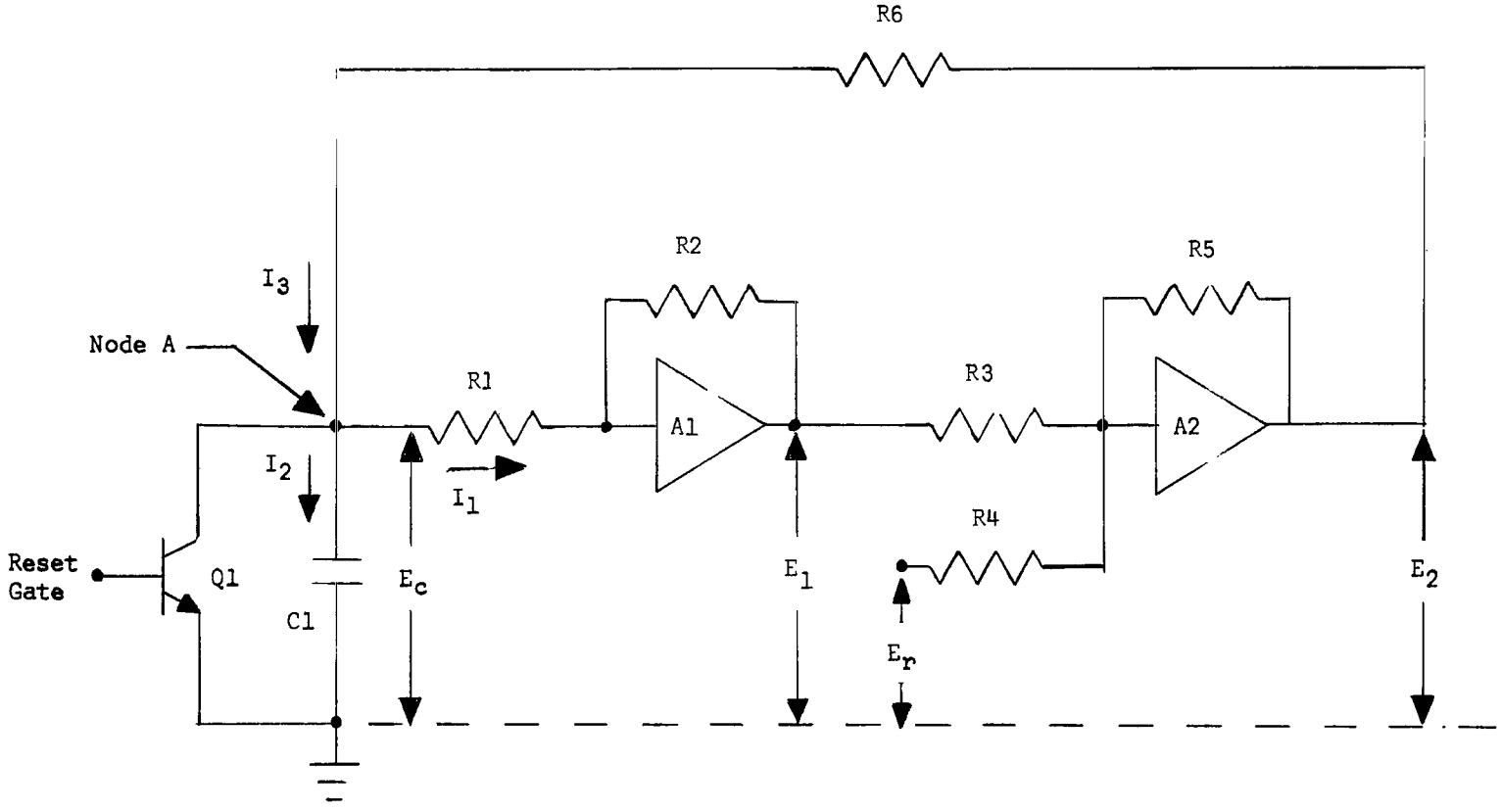

Figure 15.- Voltage sawtooth generator.

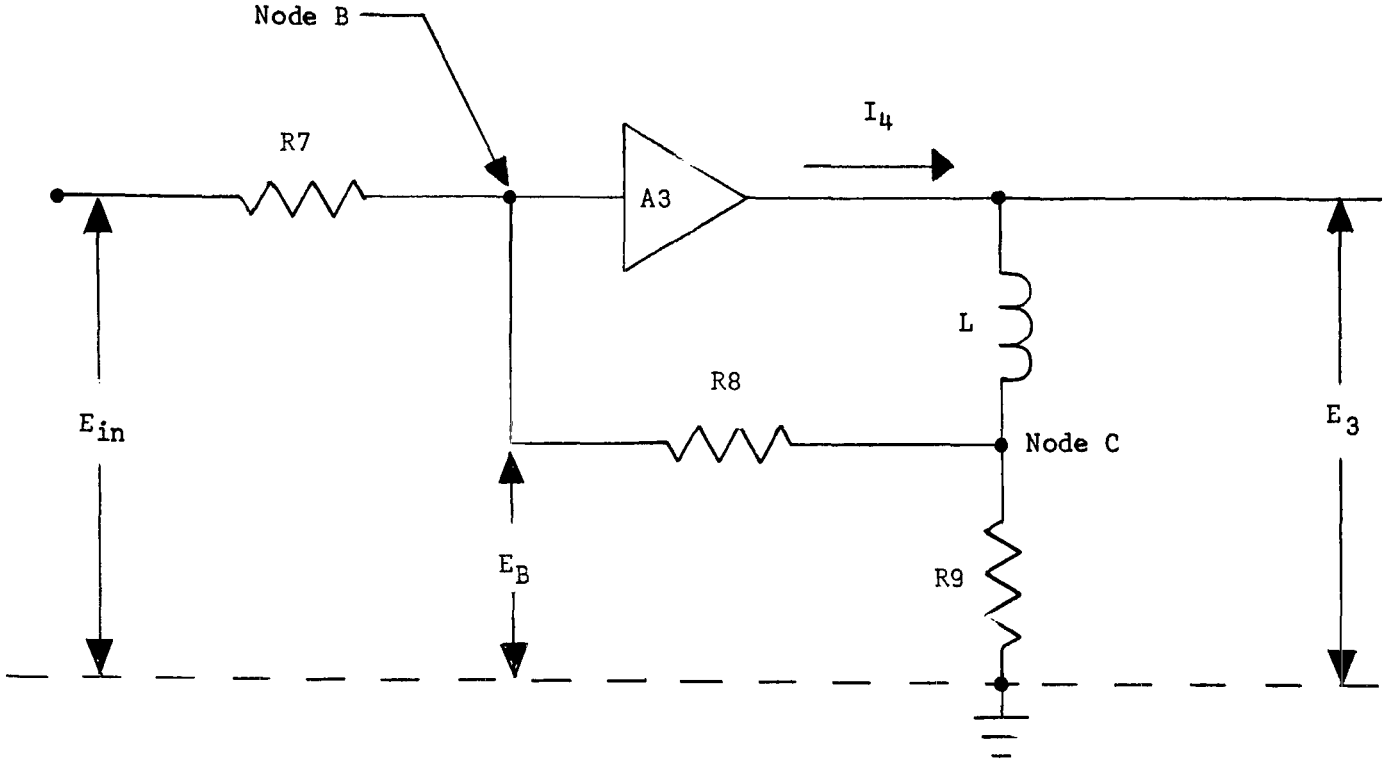

Figure 16.- Deflection amplifier.

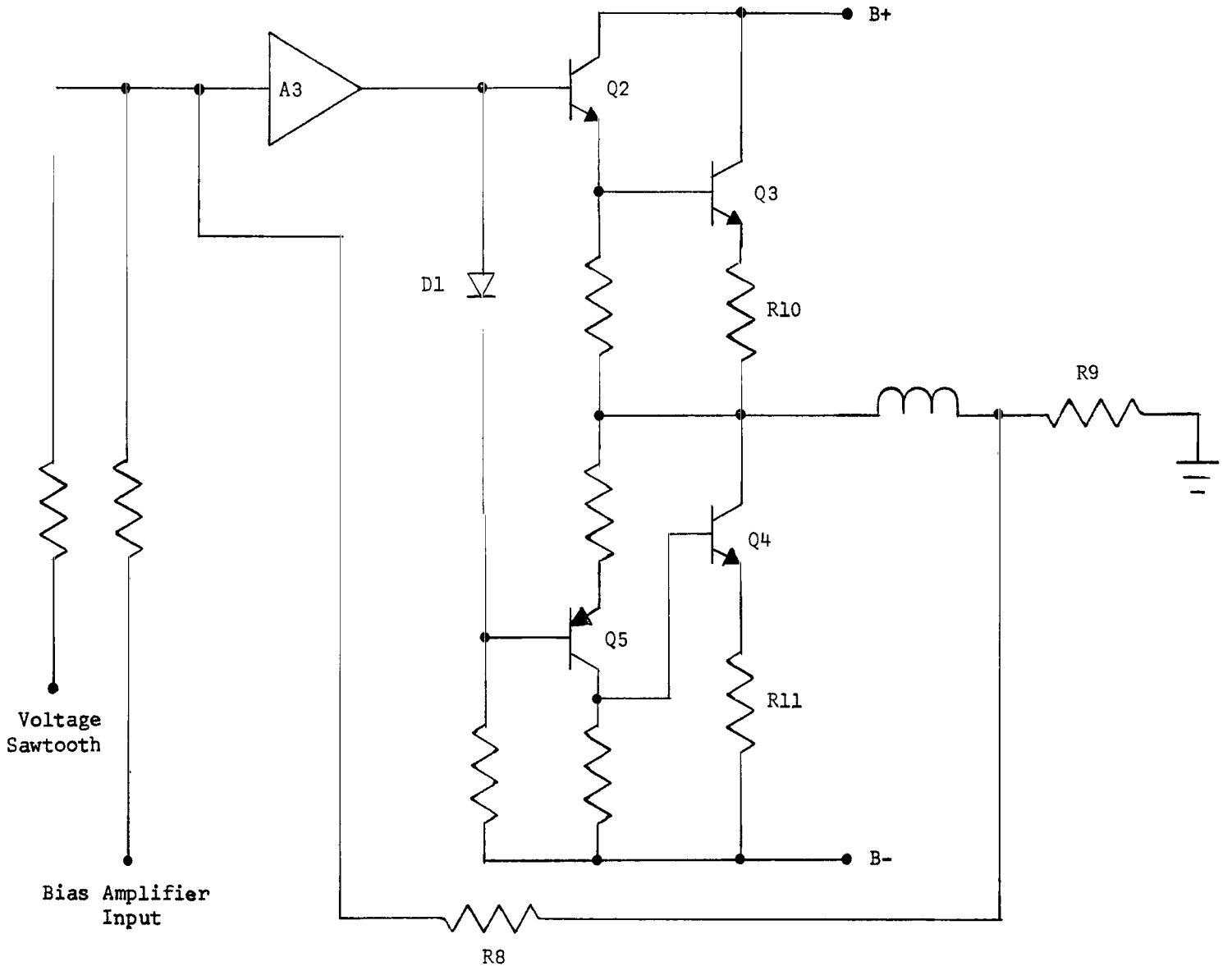

Figure 17.- Power amplifier.

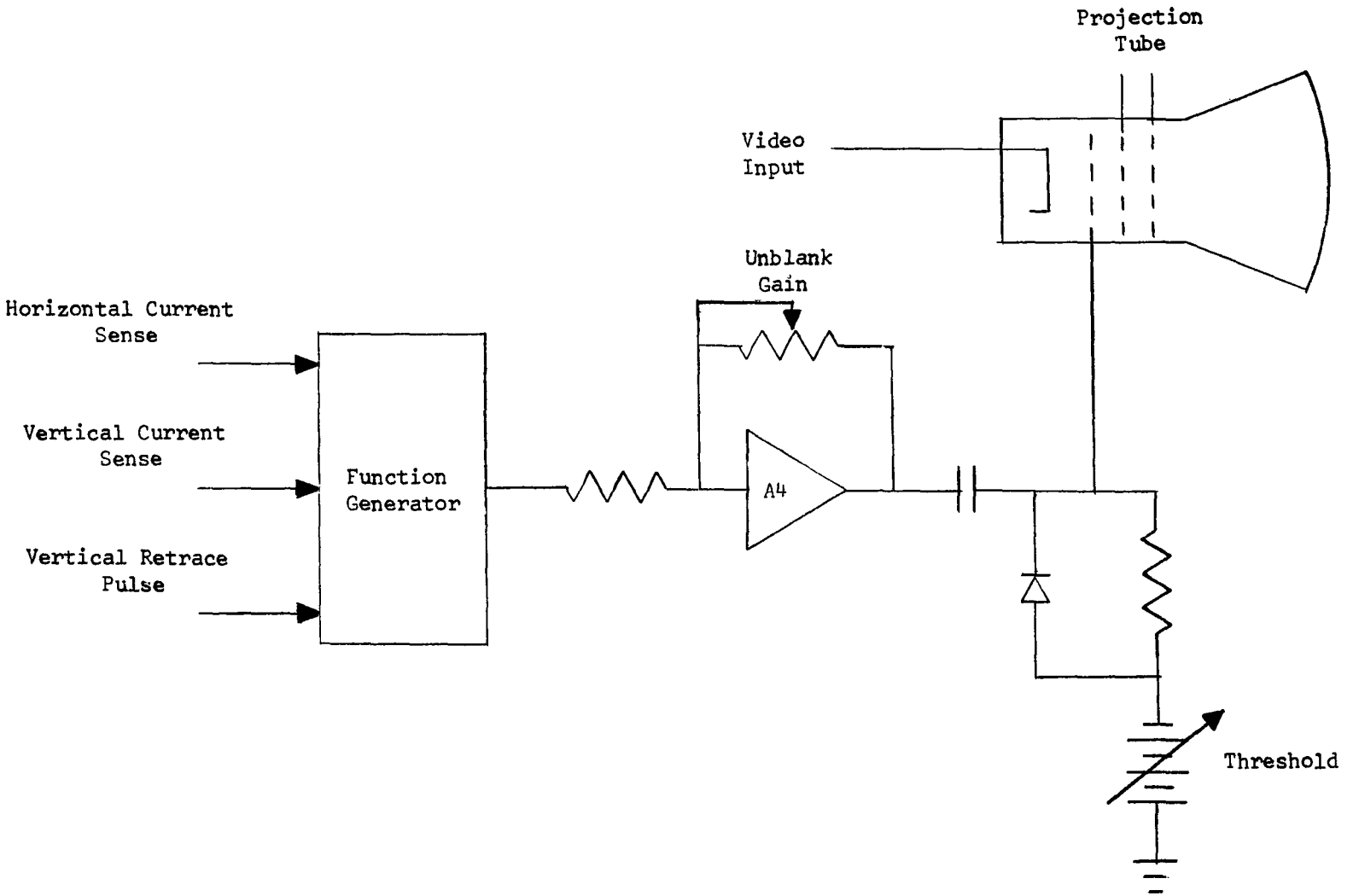

Figure 18.- Intensity control.

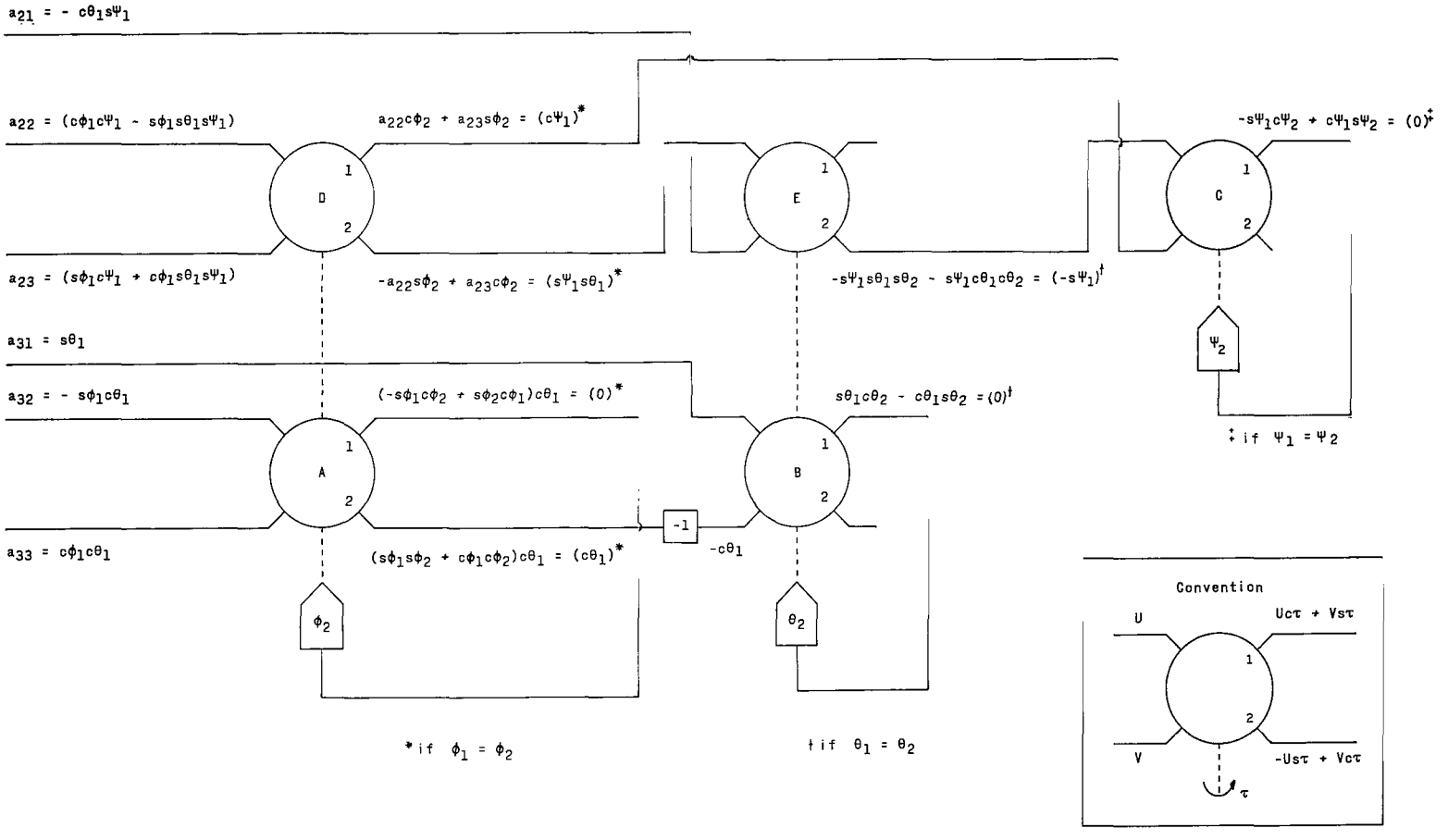

Figure 19.- Euler angle computer mechanization.

NATIONAL AERONAUTICS AND SPACE ADMINISTRATION
WASHINGTON, D. C. 20546

OFFICIAL BUSINESS

FIRST CLASS MAIL

POSTAGE AND FEES PAID
NATIONAL AERONAUTICS AND
SPACE ADMINISTRATION

POSTMASTER: If Undeliverable (Section 158 Postal Manual) Do Not Return

"The aeronautical and space activities of the United States shall be conducted so as to contribute . . . to the expansion of human knowledge of phenomena in the atmosphere and space. The Administration shall provide for the widest practicable and appropriate dissemination of information concerning its activities and the results thereof."

—NATIONAL AERONAUTICS AND SPACE ACT OF 1958

NASA SCIENTIFIC AND TECHNICAL PUBLICATIONS

TECHNICAL REPORTS: Scientific and technical information considered important, complete, and a lasting contribution to existing knowledge.

TECHNICAL NOTES: Information less broad in scope but nevertheless of importance as a contribution to existing knowledge.

TECHNICAL MEMORANDUMS: Information receiving limited distribution because of preliminary data, security classification, or other reasons.

CONTRACTOR REPORTS: Scientific and technical information generated under a NASA contract or grant and considered an important contribution to existing knowledge.

TECHNICAL TRANSLATIONS: Information published in a foreign language considered to merit NASA distribution in English.

SPECIAL PUBLICATIONS: Information derived from or of value to NASA activities. Publications include conference proceedings, monographs, data compilations, handbooks, sourcebooks, and special bibliographies.

TECHNOLOGY UTILIZATION PUBLICATIONS: Information on technology used by NASA that may be of particular interest in commercial and other non-aerospace applications. Publications include Tech Briefs, Technology Utilization Reports and Notes, and Technology Surveys.

Details on the availability of these publications may be obtained from:

SCIENTIFIC AND TECHNICAL INFORMATION DIVISION

NATIONAL AERONAUTICS AND SPACE ADMINISTRATION

Washington, D.C. 20546